

Chapter 2

THE ORIGINS OF SPACE WEATHER

2.1 INTRODUCTION

In this chapter, we turn our attention to the solar-terrestrial environment. We examine the rudiments of solar structure and processes, the genesis and consequences of solar activity, the solar wind and the interplanetary magnetic field (IMF), elements of relevant magnetospheric processes, and solar-terrestrial relationships. We cover solar activity cycles and indices and their importance in specified prediction systems. Relevant prediction systems and services are covered in Chapter 5.

The first title of this chapter was “The Anatomy of Space Weather”, but it was changed for several reasons. First of all, the term anatomy suggests a precise dissection of the various processes on the sun and its environment that lead to space weather phenomena. Our real intent is to provide a relatively short overview of such phenomena to the extent they are relevant to our real objective, that of understanding the impact upon telecommunication systems. Moreover there are numerous books that detail solar physics, and these details need not be repeated here. Secondly, it has been noted that up to 70% of space weather occurs in the ionosphere [Meier, 2000]. It certainly appears logical to place the sun and its importance *up front* in this particular book, but it is also sufficient to present the topic in summary fashion, since we dare not diminish the role of the ionosphere that should be at the heart of any dissertation on space weather. Having dispensed with this rationalization for an abbreviated treatment of the sun and space weather origins, let us proceed.

In recent years, the importance of the corona, including coronal holes and coronal mass ejections (i.e., CMEs), has emerged. Certainly a treatment of these phenomena is needed to grasp the impact of transient phenomena that tend to dominate methods of short-term forecasting. An associated phenomenon of major importance is the geomagnetic storm. This topic is central to the matter of any intermediate ionospheric forecasting system since (i) the geomagnetic activity is strongly coupled to the ionosphere, (ii) the ionospheric response is delayed with respect to flare effects, and (iii) the impact is global and relatively long-lasting. The latter property makes the treatment of geomagnetic storms and their causal mechanisms an invaluable component of performance assessment for telecommunications systems that operate in the ionospheric environment. It is duly noted that an ionospheric storm is the response of the ionosphere to a geomagnetic storm. As suggested

above, we shall intentionally limit our treatment of ionospheric storms and related disturbances in the present chapter, leaving these important topics until Chapter 3. In the present chapter we largely restrict our discussion to the origins of space weather. A discussion of new satellite observation systems and other space weather resources will be deferred until Chapter 6. The reader will find many excellent texts that deal almost exclusively with solar and magnetospheric physics, and the author will not attempt to duplicate them either in terms of scope or rigor. For detailed discussions of the sun and the magnetosphere, the bibliography at the end of the chapter should be consulted.

The importance of solar activity as it relates to telecommunication systems is well established. It is recognized that the sun exhibits sudden outbursts of energy that are called solar flares, and that these events may play havoc with the performance of certain radiowave systems including commercial television. However these events are relatively short-lived, typically lasting the order of an hour or less. Other well-known influences of the sun include those changes associated with an intensification in the extent and magnitude of the visible and radio auroras. These events affect high latitude terrestrial and earth-space communication to be sure, but the disturbances are actually global in nature. This is evidenced by the fact that ionospheric storms introduce significant alterations in HF coverage at middle latitudes, as well as enhanced scintillation of signals traversing earth-space paths. These scintillation enhancements are due to a descent of the scintillation boundary, corresponding to an equatorward expansion of the auroral zone. We shall find that solar influences on the ionosphere, may generally be characterized as immediate or delayed, with the long-term occurrence of these categories following an 11-year cycle. A well-known index of solar activity that exhibits the cyclic pattern is the sunspot number. This index roughly characterizes the number of spots on the visible solar disk, and is proportional to that component of solar activity that most severely influences telecommunication systems. The 11-year solar cycle is not subject to precise characterization in terms of onset, duration, or magnitude; and its direct influence on the ionosphere is not always clear. Nevertheless, we use indices of solar activity, or proxies of same, in all current long-term prediction programs. The role of ionospheric models is covered in Chapter 3 and prediction systems are covered in Chapter 5.

The ionosphere owes its existence to the sun, but it would clearly exist even in the absence of the 11-year cycle of sunspots. Indeed, the ionosphere possesses some rather interesting features even during periods of few sunspots. Without the 11-year modulation of activity, the ionosphere would possess a reasonably deterministic variability, which is associated with the local solar zenith angle, including diurnal and seasonal effects that are

appreciably controlled by geometry. Moreover, even the benign ionosphere is characterized by relatively unpredictable variations that arise because of the constitution and dynamics of the underlying neutral gas. In fact there are a host of temporal fluctuations, which originate from sources other than the sun including neutral atmospheric weather patterns and turbulence. This, of course, does not suggest a lack of ultimate linkage to the sun. In any case, this residual class of fluctuations poses interesting challenges for ionospheric forecasting specialists who have long concentrated on the more obvious and direct association between the sun and the ionosphere.

2.2 THE SUN AND ITS INFLUENCE

Following the tradition of many monographs dealing with radiowave propagation and texts on magnetospheric and ionospheric physics, we shall include a review of the nature of solar activity. However, since we are ultimately interested in telecommunication disciplines and not solar physics, our treatment will exclude the more esoteric topics and consider mainly those issues that will provide an insight for the telecommunication specialist.

2.2.1 Solar Structure and Irradiance Properties

A qualitative picture of the modes of outward energy flow from the sun is given in Figure 2-1. The source of solar activity lies within the central core region. The process by which the energy is generated within the core is similar to the mechanism exploited in the detonation of fusion weapons, but in the case of the sun these reactions are hidden from us because they are constrained by the enormous gravitation pressure of the overlying solar layers.

Figure 2-2 depicts the complex structure of the sun and shows a number of the features that have been studied by solar scientists as well as by engineers involved in the prediction of ionospheric impact on terrestrial systems. Solar physicists now have a good understanding of many of the basic characteristics of the sun, including its average temperature, mass, size, constituents, etc. The sun is about 93 million miles from the earth, it has a mass of about 330 thousand earths, it is a gaseous body, and it rotates (from left to right as viewed from the earth) with a period of about 27 days.

The sun is composed of 90% hydrogen and 9% helium, the latter being formed by the fusion of hydrogen, and 1% heavier trace elements. The energy-producing fusion reactions occur in the central core region, generating a temperature of approximately 10 million degrees Kelvin (°K). The energy from the fusion reactions takes 1 million to 50 million years to reach the solar surface.

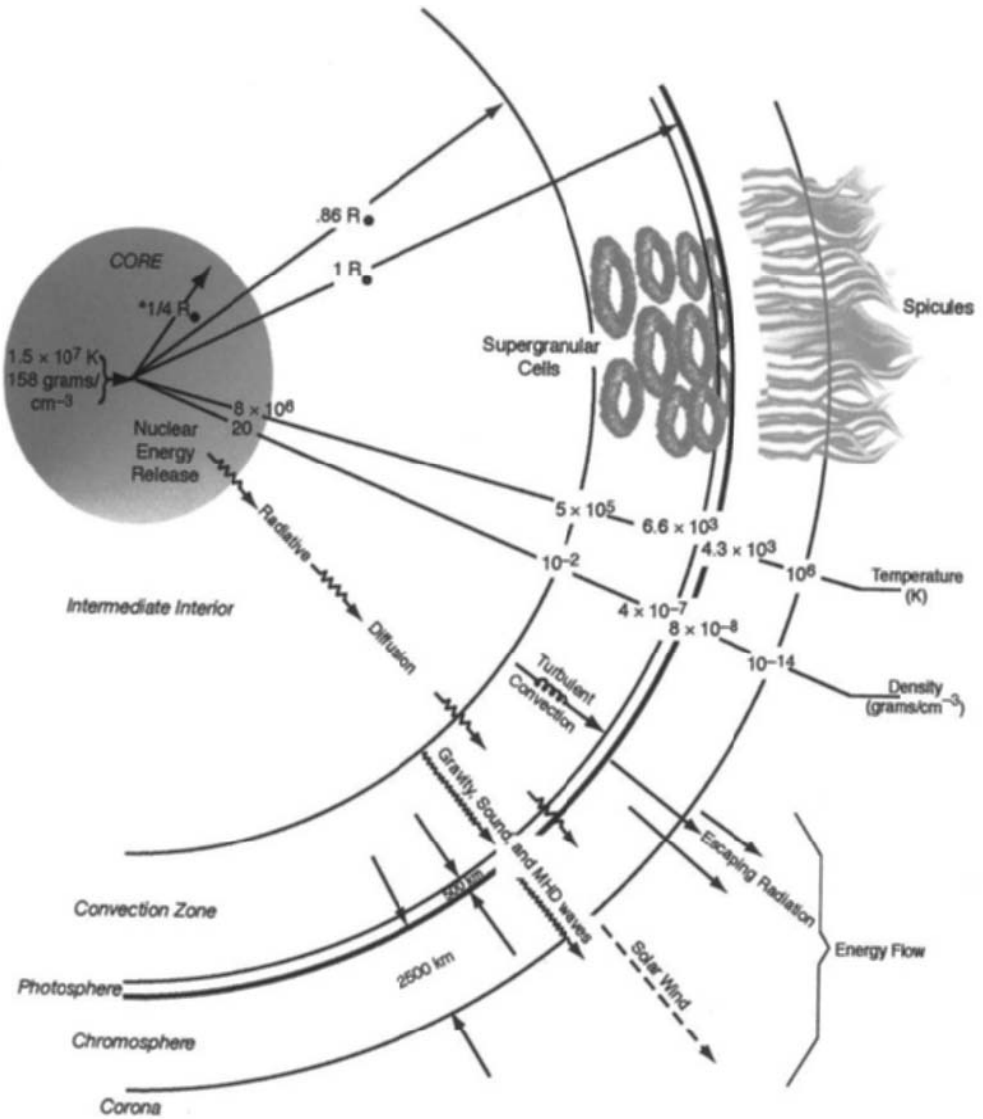


Figure 2-1: A model of energy flow from the sun. Shown are the temperature, density, and phenomenological profiles. The central core region is the seat of energy production. The major zones in the outer region (i.e., $> 0.86 R_s$) include the convection zone, the photosphere, the chromosphere, and the corona. The corona is observed with a coronagraph or during a solar eclipse. The personality of the corona is of major significance in space weather predictions. Adapted from Jursa [1985]

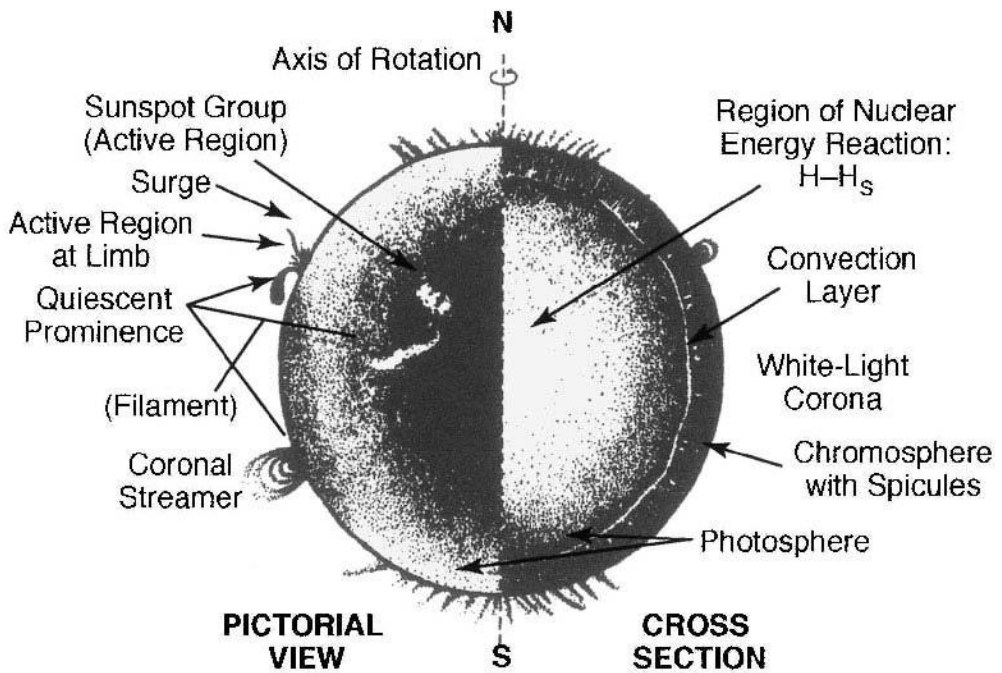


Figure 2-2: Cartoon showing principle features on the sun. Regions are not to scale. Refer also to Figure 2-1. Adapted from Goodman [1991], after Valley [1965].

As observed in Figure 2-1, the temperature of the solar regions diminishes from millions of degrees in the core to its minimum value of several thousand degrees in the lower chromosphere. It rises again to roughly a million degrees in the tenuous solar corona. The equivalent blackbody temperature of the photosphere of the sun is about 6000 °K for electromagnetic wave emissions having wavelengths less than 1 cm. Solar images taken with different wavelengths can be associated with different altitudes. From the photosphere, both UV and visible radiation is emitted. The energy associated with a gas having a temperature T is given by:

$$E \cong kT \quad (2.1)$$

where k represents Boltzmann's constant = 1.38×10^{-23} J/°K, T is the absolute temperature (°K), and E is in Joules (J).

Typically workers use electron volts (eV) as a measure of the energy. One electron volt is the energy of an electron that has been accelerated through a potential difference of one volt. In terms of electron volts we use the following transformation:

$$V = E/q \tag{2.2}$$

where V is the equivalent energy in electron volts (eV), E is the energy (J), and q is the charge of an electron = 1.6×10^{-19} Coulombs.

Wien’s Displacement Law allows one to determine the wavelength corresponding to the maximum radiation in the spectral distribution. We have:

$$\lambda = 2.9 \times 10^{-3} T^{-1} \tag{2.3}$$

where λ is in meters, and T is the absolute temperature. As the temperature goes to higher levels, the wavelength decreases, and, of course, the frequency increases. Table 2-1 is a listing of wavelengths, and energy levels corresponding selected values of gas temperature. One can convert to frequency using the relation $\lambda f = 300$, where f is in MHz and λ is in meters.

Table 2-1: Temperature, Energy, and Wavelength and Spectral Designation

Temperature (⁰ K)	Energy (eV)	Wavelength (10 ⁻⁹ m)	Spectral Designation
1000	0.1	2900	Infrared
7000	0.6	414	Visible
10,000	0.9	290	Ultraviolet
70,000	6.0	41	Extreme Ultraviolet
700,000	60	4	soft x-rays

Solar radiation can be categorized either as thermal (and broadband) or as line spectral radiation. The line spectra arise as extra-nuclear electrons adjust their positions (and energy levels) following collisional ionization from an electron-atom interaction.

At one time it was thought that the integrated electromagnetic flux from the sun as reckoned at a fixed distance from the solar surface was a constant. However, even correcting for earth-sun distance variation, the solar constant, which is a measure of the total solar irradiance at a distance of one astronomical unit (1 a.u.), has been found to fluctuate slightly. Its value is approximately 1370 watts/m². Figure 2-3 illustrates the relative importance of selected bands in the electromagnetic spectrum.

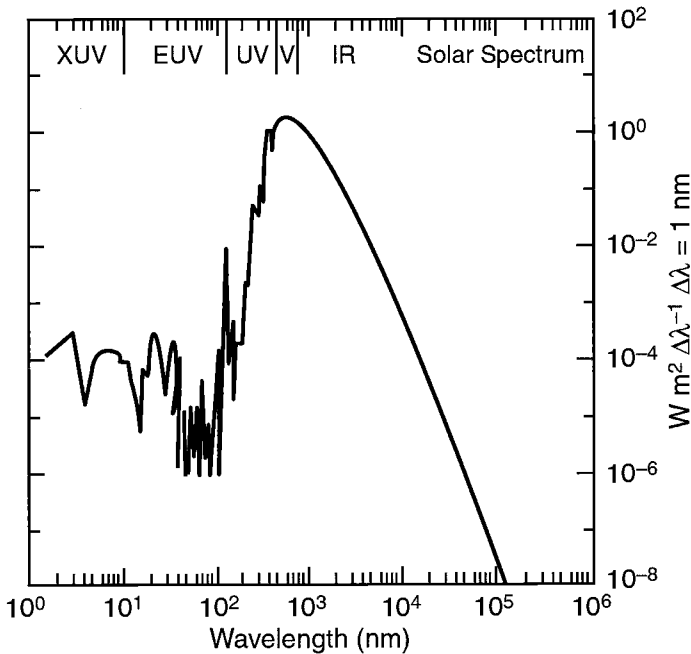


Figure 2-3: The solar spectral distribution from the x-ray band through the radio band. The plot represents irradiance (watts/m^2) versus wavelength (nm) where the irradiance is normalized to a wavelength increment of 1.0 nm. Increasing wavelength is to the right, and increasing energy/photon is to the left. The numbers represent approximate percentages of the solar constant, $H \sim 1366 \text{ watts/m}^2$. The visible spectrum is between 400 and 700 nanometers (nm), where $1 \text{ nm} = 10^{-3} \text{ microns}$. The irradiance curve is adapted from data due to Space Environment Technologies.

The largest contribution to solar irradiance variability (in percentage rather than absolute terms) may be found on the extremes of the spectrum exhibited in Figure 2-3. These regions of greatest variability (i.e., the radio region and the x-ray region) have the most profound effect on the constitution of the upper atmosphere and the ionosphere. Unfortunately, for the purpose of observational science, but fortunately, for purposes of biological safety, a large proportion of the high-energy component corresponding to the ultraviolet (UV), extreme ultraviolet (EUV) and x-ray bands (XUV) is strongly absorbed in the atmosphere. The radio components are virtually unaffected.

EUV and x-ray components are quite influential in photoionization processes, and the UV component is related with ozone layer production. The low energy component of spectral irradiance corresponding to the radiowave

region provides information about energetic particle events and about the general level of solar activity. In fact radio data at 10.7 cm (2800 MHz) may be used as a measure of solar activity since such data is more reliable (and perhaps more meaningful) than the well-known sunspot number. Space Environment Technologies, a commercial firm specializing in irradiance measurements and forecasts, finds that the solar constant, S , changes slightly over time and the currently accepted value is $\sim 1366 \text{ W/m}^2$.

Solar physics is a complex subject and many of the fundamental solar phenomena are still incompletely understood. Therefore, at the present time, the important components of electromagnetic and corpuscular flux exiting the sun would appear to exhibit a degree of chaotic behavior. This chaotic behavior is exclusive of more familiar tendencies toward regularity in the temporal pattern of radiation; especially those phenomena associated with the solar rotation period (27 days), and the 11-year solar cycle of sunspot population. As would be expected, the regular patterns are more amenable to prediction. Nevertheless, the chaotic behavior generally controls the short-term environment making near-term forecasts of solar behavior difficult. Moreover, a clear relationship between a particular solar event and its properties (the cause) and the terrestrial disturbance (the effect) is generally lacking. This has a profound effect upon our ability to predict ionospheric behavior and, of course, telecommunication performance.

Because of the circumstantial relationship existing between sunspot number and ionosphere state, considerable effort has been directed toward the development of sunspot number prediction methods. Various prediction methods have been reviewed by Withbroe [1989]. Neural networks have been used to provide estimates of the maximum number of sunspots and when the maximum level will occur [Koons and Gorney, 1990].

2.2.2 On the Nature of Solar Activity and Sunspots

Solar physics provides a basis for our comprehension of solar phenomena, and we use this knowledge to explain previous solar events or to forecast future activity. The relationship between sun and earth is of profound importance for a variety of reasons. An unequivocal linkage between certain solar phenomena and the ionospheric state was established decades ago, largely the result of ionospheric measurements using HF sounders, incoherent scatter radars and rocket probes. More recently, advanced satellite observation platforms has made the case even stronger. Herbert Friedman's *Sun and Earth* [1985] is recommended for additional reading.

To study the origin of sunspots, it is necessary to examine the magnetic field structure on the sun, because, in the absence of the solar magnetic field, current theory does not explain the generation of sunspots or

their cyclic behavior. To first order, the sun's field is oriented N-S in its quiescent configuration (sunspot minimum), and its intensity is little more than that of the earth's magnetic field, being approximately 1 gauss. However, the sun differs from the earth, where the primary source of the field is within the metallic core, because the solar field is confined near the surface. The field is *frozen-in* to the surface plasma that can move, transporting the field lines with it. In short, the magnetic field is generally too weak to extricate itself from the control of the highly ionized solar plasma. Since the sun and its surface plasma rotate about its NS axis, co-rotation of the surface magnetic field also occurs. However, since the sun is a fluid, this rotation is not uniform as a function of solar (or heliographic) latitude. Indeed, the solar surface rotates differentially, with the equatorial region moving more rapidly than higher heliographic latitudes. This causes the solar magnetic field to become wrapped around the sun over a period of time. It also increases the equatorward magnetic field. Eventually the neighboring stretched field lines become intertwined because of turbulent motion originating in the underlying convection zone. Figure 2-4 shows how this happens. The twisted field lines are hidden below the visible surface and the most intense regions are associated with local magnetic fields of about 4000 gauss. Such fields exert enormous magnetic pressure on the surrounding plasma. As the magnetic pressure begins to exceed the plasma pressure, the fields penetrate the surface and appear as bipolar loops. This phenomenon arises first at a solar latitude of ~ 40 degrees where the field line stretching and convergence is most intense. At the points where the field lines protrude from the surface, the magnetic field intensity is so large that energy is prevented from reaching the surface. These points of opposite polarity are several thousand degrees cooler than their surroundings and appear as dark spots on the photosphere.

Sunspot pairs usually occur in large groups and are contained within rather long-lived (calcium plage) regions. The *preceding* sunspots of the sunspot pairs have the same polarity as the pole of their hemisphere, whereas the *following* sunspots have the opposite polarity. Because of differential rotation, the *following* sunspots lag the overall group motion and form distended unipolar regions that gravitate toward the pole. As a result the latitude of maximum stress moves equatorward and the polar fields become eroded. At sunspot maximum, the polar fields have become completely neutralized. Beyond this point in time, the pole reversal process begins, and the amount of sunspots, now being formed near the low latitude region of limited differential rotation, begins to wane.

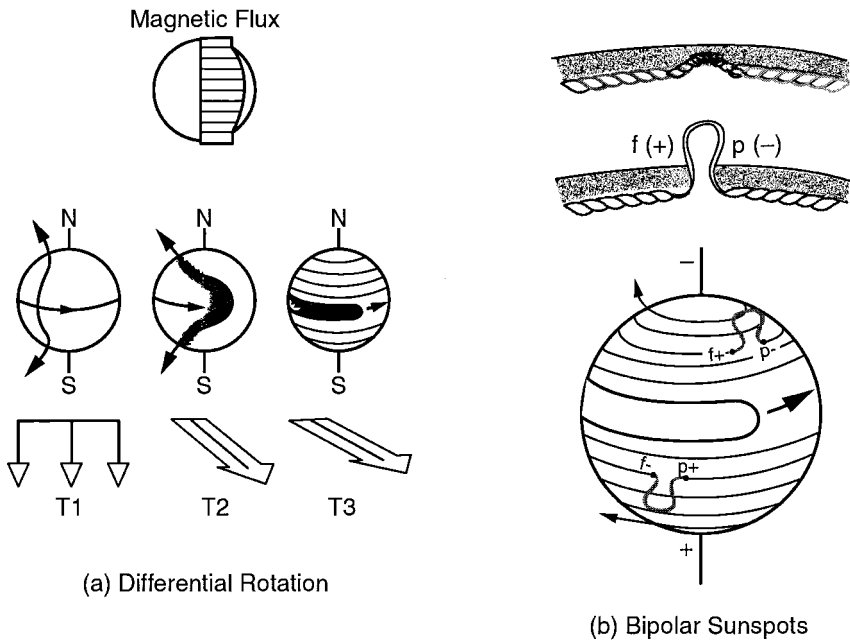


Figure 2-4: Effects of differential rotation on the sun: (A) Development of east-west component of the surface field as the field lines become stretched out between the times T_1 , T_2 , and T_3 . This brings the lines of magnetic flux closer together. (B) Formation of kinks in the plasma field configuration, leading to the development of bipolar sunspots. An eventual reversal of the field at the poles results from the effective poleward migration of the following spots, which have an algebraic sign opposite to that of the pole in their hemisphere. Adapted from Gibson [1973].

By the time the polarity of the magnetic field has completely reversed, no sunspots are evident. Near solar minimum, the field lines that had been intertwined return to a mostly longitudinal (i.e., N-S) configuration. It takes about 11 years for this process to be completed, and it takes about 22 years for the original magnetic configuration to recur. The process is shown in Figure 2-5. From the figure, we see that the spots first start to appear below 40 degrees latitude, both north and south. The maximum solar activity, as represented by the sunspot area index, occurs several years after sunspots first emerge and several years before the last sunspots appear near the equator.

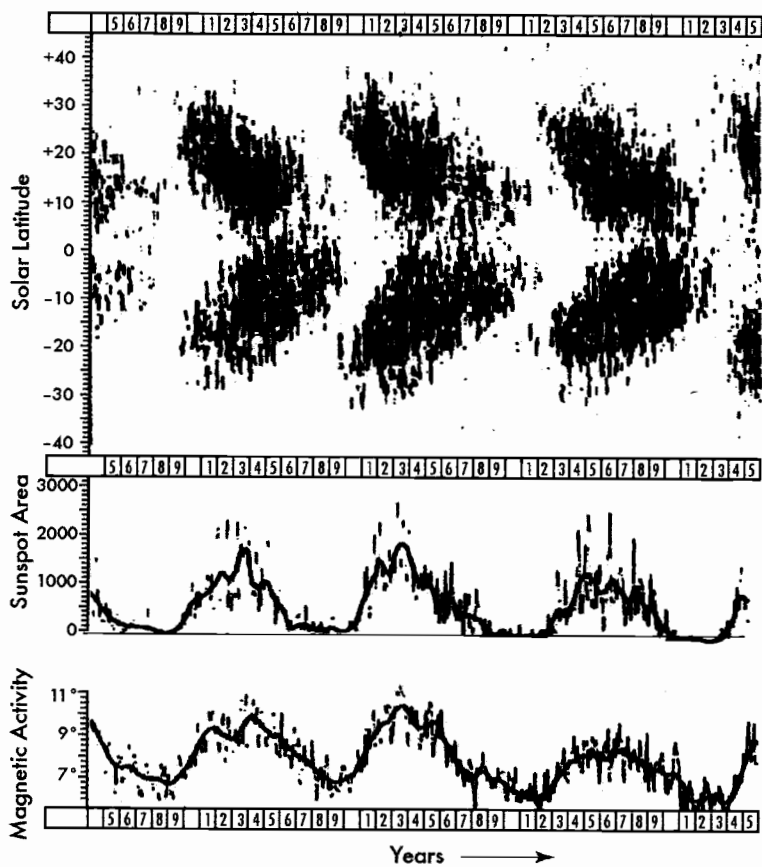


Figure 2-5: The top curve is a so-called *Butterfly diagram*, which shows the migration of sunspots from high latitudes to low as the solar cycle progresses. Also shown is the area of sunspots (middle plot) and a measure of magnetic activity (bottom). Adapted from Chapman [1968].

2.2.3 Active Regions, Coronal Holes, and the Solar Wind

Active areas on the sun are the regions where there arise many phenomena whose form depends upon the region of the spectrum being monitored. Sunspots are best observed in the visible wavelengths, whereas disturbances in the coronal area overlying the disk are best examined in the soft x-ray band with satellite or rocket-borne instruments that are not affected by atmospheric absorption. X-ray emissions are not observable at ground level, and white light observations of the tenuous corona are made problematic by the overwhelming brightness of the solar disk.

The earliest measurements of the solar corona were made during solar eclipses or by using a special instrument called a coronagraph. By superposing successive limb scans, it has been possible to reconstruct an image of coronal disturbances in the visible part of the spectrum. While this method does not generate a frozen picture in time (i.e., a snapshot), it allows coronal observations to be mapped over the entire disk area. The first direct x-ray and UV maps of coronal disturbances were made using rocket probes, but it remained for instruments aboard the Skylab satellite to produce the first comprehensive observations of these disturbances and call attention to coronal holes.

What is a coronal hole? Employing a coronagraph, the visible manifestation of a coronal hole is a lack of coronal brightness in certain regions surrounding the disk; this diminution usually arises and persists near the solar poles. These regions, termed coronal holes, are not devoid of plasma but the density is much less than that found in the surrounding gas. These holes are coupled to underlying unipolar active regions where the field lines are nearly radial. Such a configuration allows plasma to escape the sun and propel itself into space. The observation of coronal holes near the north and south poles of the sun is not surprising, since field lines are naturally vertical in those regions. The existence of coronal holes at low latitudes is a direct result of the generation of bipolar sunspots, progressively in the equatorward direction, and the growth of large unipolar regions. Figure 2-6 shows a coronal hole, which was observed from the Skylab x-ray telescope. This hole extended from the North Polar Region into the southern hemisphere, and was persistent in this general form for over six 27-day rotations of the sun. Through a hole of this type, solar plasma has an escape route similar to that which it has from the polar region.

It is thought that the original notion of a continuous stream of plasma emanating from the sun was born in the early 1950s, based upon comet tail deflections. Subsequently, E.N. Parker [1959] first coined the term *solar wind* to refer to the logical expansion of the solar corona. Solar wind plasma that escapes from the sun carries a signature with it, the embedded magnetic field that may be either sunward or anti-sunward. This coronal magnetic field is transported by the expanding corona into interplanetary space along distended spiral arms, which are called Archimedes spirals. These spirals resemble a rotating gardenhose. They appear as spirals for the following reason. Initially, the solar magnetic field is dominant within the corona causing an initial corotation of the exiting plasma. However, with increasing distance from the sun, the kinetic energy of the plasma will gradually dominate the magnetic field energy resulting in a lag in rotational component of plasma motion. Hence, the expanding coronal plasma appears to fall behind with respect to the rotation solar disk. Parker's solar wind transports the solar magnetic field,

known as the Interplanetary Magnetic Field (IMF), throughout the heliosphere.

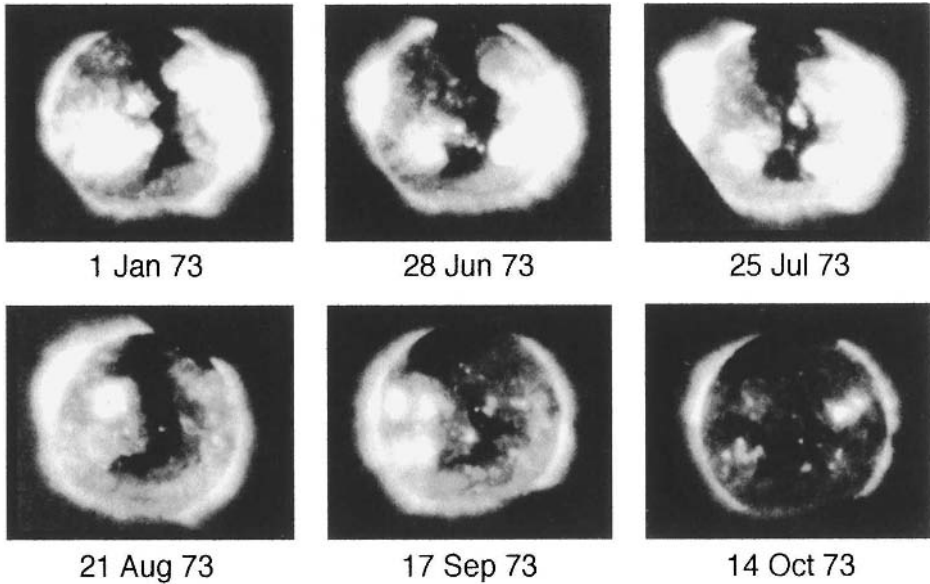


Figure 2-6: Example of a coronal hole observed with Skylab. This event occurred during the decreasing portion of solar cycle 20. Each photograph is separated from its neighbor by 28 days, the average period of a solar rotation. Selected photographs are taken from Figure 1-29 in the Air Force Handbook [Jursa, 1985].

Returning to the sun, we usually find that the predominant magnetic field polarities within the large unipolar regions in the southern and northern solar hemispheres have opposite signs. Opposing fields from the large unipolar regions tend to reconnect at a great distance from the sun producing a neutral sheet in the neighborhood of the ecliptic plane. Looking down on the pole, a sector structure of the IMF is observed, with the magnetic field polarity in adjacent sectors being reversed. This interesting feature is the result of a latitudinal undulation in the neutral current sheet that, under quiescent conditions, would reside in the neighborhood of the ecliptic. The solar wind speed is greatest away from sector boundary crossings. Wind speeds may vary from 700 km/sec during disturbed times and within the center of a sector, to 300 km/sec in the neighborhood of a sector boundary crossing. Greater wind speeds cause more significant ionospheric effects.

Measurements of the IMF and the solar wind speed are useful for the derivation of indices for estimating ionospheric effects. Missions such as Ulysses, IMP-8, ISEE and WIND have shed considerable light on the subject and the ACE satellite is now providing operational data. Some research has suggested that scintillation of selected interstellar radio sources (using measurements made by ground-based radio telescopes) may be associated with the plasma density inhomogeneities within the solar wind. More information regarding ACE may be found in Chapters 5 and 6.

Solar wind speed and IMF characterization are both important in the ultimate impact on the magnetosphere and underlying ionosphere. Solar wind speeds vary, as do magnetic field orientations. It has been demonstrated that the solar wind speed associated with coronal holes is generally much faster than the average solar wind speed. Table 2-2 provides some data on solar wind properties:

Table 2-2: Representative Solar Wind Properties

Solar Wind Parameter	Minimum	Average	Maximum
Flux (particles $\text{cm}^{-2}\text{sec}^{-1}$)	1	3	100
Speed (km sec^{-1})	200	400	900
Density (particles cm^{-3})	0.4	6.5	100
Magnetic Field, B (nT)	0.2	6	80

2.2.4 The Canonical Sunspot Cycle

Sunspots are indicators of other phenomena that can be important to space weather, and ultimately to ionospheric effects on telecommunication systems. Actually, sunspots are probably overrated as indicators of space weather phenomena. Nevertheless, sunspots have been monitored for centuries and have proved to be a useful if imprecise index. Indeed, because of its historical record and availability, most predictive models are at least partly based upon some measure of the sunspot number.

The most common index of solar activity is based upon a count of the number of sunspots on the solar disk. The fundamental index is the relative sunspot (or Wolf) number that is reckoned daily. It is given by the following relationship developed by Rudolf Wolf who was the first director of the Swiss Federal Observatory in Zurich:

$$R = k(10g + s) \quad (2.4)$$

In Equation 2.4, k is a correction factor dependent upon the observatory, g represents the number of sunspot groups, and s is the number of individual spots. For many years the Wolf number was compiled from measurements

compiled at Zurich. Until 1981, when it was discontinued, it formed the basis for many solar and ionospheric studies. After 1981, the Zurich number (termed R_Z) was replaced by the International sunspot number, R_I . About 25 stations are involved in the construction of R_I . Throughout the chapter we will use the term SSN as a generic for various forms of sunspot number, including R_Z and R_I .

Records of daily and averaged sunspot numbers are archived by the World Data Center A for Solar-Terrestrial Physics through the National Geophysical Data Center located in Boulder, Colorado. The Solar Influences Data Center (SIDC) in Brussels, also a Regional Warning Center, compiles the International Sunspot number and various other products (See Chapter 5).

Another index of solar activity used by many because of its ease of determination and its power as a representative index of solar activity is the noontime value of the 10.7 cm (i.e., 2800 MHz) solar flux, ϕ , from either the Penticton Radio Observatory or from Ottawa. This index is expressed as a monthly mean value in units of 10^{-22} Watts m^{-2} Hz^{-1} . Stewart and Leftin [1972] have compared the Ottawa flux index with the sunspot number and have derived the following relationship:

$$\phi_{12} = 63.7 + 0.728 R_{12} + 8.9 (10^{-4}) R_{12}^2 \quad (2.5)$$

where ϕ_{12} and R_{12} are the 12-month running mean values of ϕ and R respectively. Note that at solar minimum, the flux level is not zero. For a sunspot number of 100, the solar flux would be ~ 145 according to the Equation 2.5 approximation.

Figure 2-7 gives the range of daily variability in the sunspot number for a period of 170 years, and Figure 2-8 exhibits the 10.7 cm (2800 MHz) solar flux from 1947-2003. Both day-to-day and month-to-month variability in both ϕ and R may be significant; but is it important from a practical standpoint? We will explore this matter in Section 2.2.6. But first we will mention a few things about prediction of the sunspot cycle.

2.2.5 Prediction of the Sunspot Cycle

All techniques used for long-term prediction of sunspots have significant error bars, and, because of this, the value of long-term predictions is questionable for any detailed propagation analysis or a meaningful evaluation of telecommunication impairments. While system performance assessment and system design factors both depend upon solar activity, long-term predictions are of more value in the latter instance. Other matters such as station-keeping, orbital decay probability, and spacecraft charging, which depend upon sunspot number at some level, can influence design parameters.

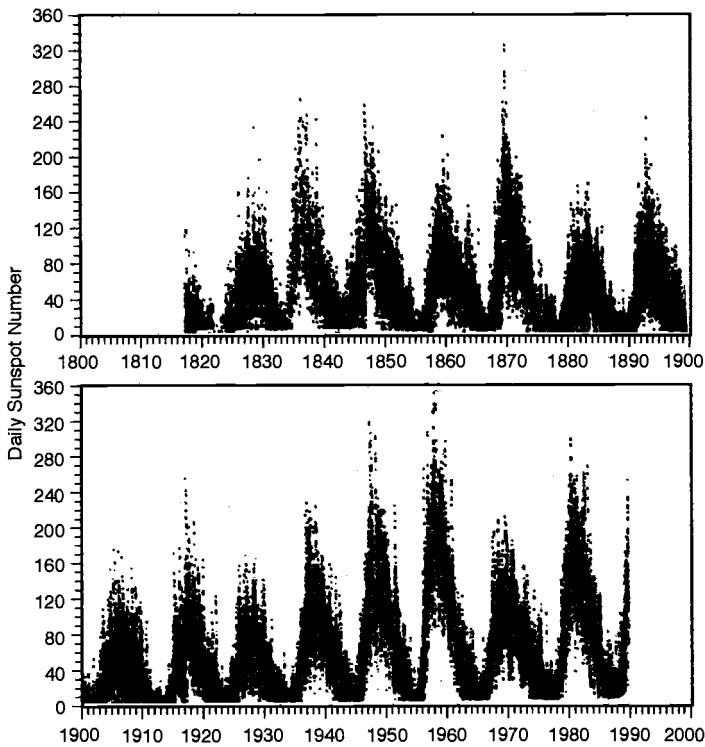


Figure 2-7: The variation of the daily sunspot number from January 1881 to January 1989. Curve is adapted from *EOS Trans, AGU*, vol.70, No. 32, 1989.

These parameters might include the fade margins and link parameters that must be imbedded in the engineering of specified telecommunication systems. Predictions might also be useful for estimating the anticipated level of impairments years in advance by associating outages incurred in the past under the same conditions as predicted. Long-term planning for military exercises could exploit good information regarding the 11-year cycle. But how good are we at doing this?

A number of methods have been used to evaluate future sunspot cycles and no method is very precise. There are several metrics to consider, including the accuracy in prediction of the maximum amplitude, the time of the maximum, and the general shape of the cycle. For the solar cycle 23, workers at NASA have examined this problem and have predicted a maximum value of 154 ± 21 , whereas the maximum of the running average was observed to be ~ 125 , slightly below the margin of error. A panel of experts organized by NOAA-SEC, and sponsored by NASA, produced a

report entitled *Solar Cycle 23 Project: Summary of Panel Findings* [Joselyn et al., 1996]. Without going into a description of the methods, Table 2-3 gives the range of values for the various techniques, and the consensus prediction, according to the panel.

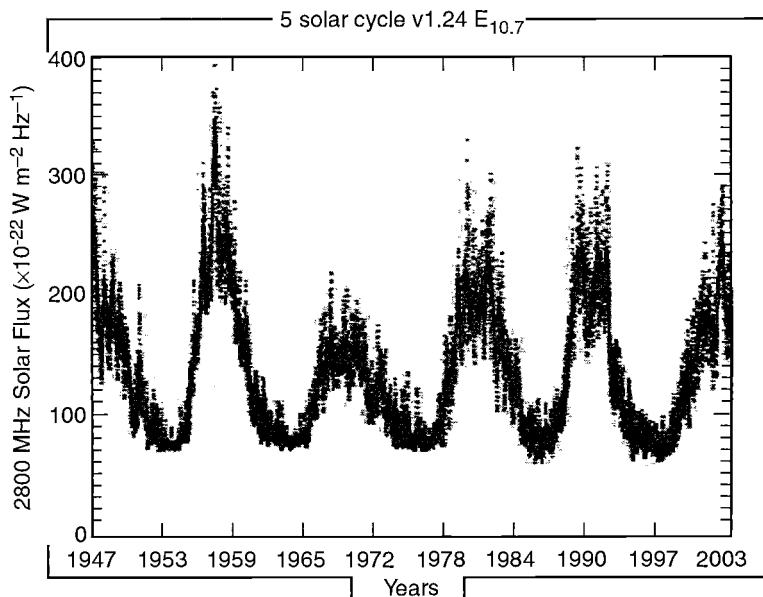


Figure 2-8: Five solar cycle pattern of the 10.7 cm solar flux from 1947-2003. This data set is derived from the SOLAR2000 model, which was developed by Space Environment Technologies (SET). Figure is provided courtesy of Kent Tobiska of SET.

It is evident from Table 2-3 that the timing of the sunspot cycle maximum is predicted with acceptable accuracy, whereas the observed value of the amplitude (i.e., 12-month running average of spots) is outside (i.e., below) the predicted range. Of all the methods cited, the “full” climatology technique appears to be best, followed by the neural network approach. This brief discussion serves to illustrate the point that even a panel of experts can have difficulty in assembling a prediction for a future sunspot cycle before its onset.

2.2.6 Solar Variability

The solar electromagnetic and particulate flux reaching the earth exhibits considerable short-term variability, and the (long-term) time-averaged behavior tracks the general tendency, but not the detailed

morphology, of solar active regions and sunspots. This narrow bandwidth behavior is well known. As one increases the bandwidth of the observational filter, we begin to see more irregular behavior. Indeed, in the time domain, the temporal variability ranges from minutes to years.

- - -

Table 2-3: Forecast of Sunspot number for Solar Cycle 23

Technique	Low End	Maximum	High End
Even/Odd behavior	165	200	235
Precursor	140	160	180
Spectral	135	155	185
Recent climatology	125	155	185
Neural Network	110	140	170
Full climatology	75	115	155
Panel's Consensus of SSN amplitude	130	160	190
Panel's Consensus of SSN peak month	January 1999	March 2000	June 2001
Observed SSN peak	-	~ 120	-
Observed peak date	-	~ April 2000	-

Note-1: By inspection of Figure 2-9, the peak monthly value of the SSN was observed to be ~ 175 at ~ July 2000. However, the smoothed (12-month “mean”) value is seen to be ~ 120.

Note-2: Sunspot cycle 23 exhibited two “peaks” in solar activity, where the secondary peak was ~ 115 at ~ December 2001.

- - -

Figure 2-9 is the ISES solar cycle 23 sunspot number progression as of 29 February 2004. It is seen that solar cycle 24 will begin on or about January 2007.

Table 2-4 stipulates the general amplitude of sunspot variability as a function of the filter time constant, using the Wolf number as the gauge of sunspot activity. It is clear that daily values of sunspot number are far more variable than monthly values. While we should always consider the highest bandwidth information when considering real-time forecasting issues, this does not always lead to the desired result. Normally one would like to compare cause and effect using the same filter, thereby enabling an improvement in the correlation expected to exist. This strategy works well at the low-frequency (high bandwidth) end, but this yields little data of interest. We really don't care about a yearly-averaged relationship between *SSN* and *foF2*, for example. However, we would like to take advantage of the daily sunspot number and some daily index of ionospheric parameters, such as the midday value *foF2*. Unfortunately, as we infer from Table 2-4, the day-to-day variability in sunspot number is sizable, and this is not reflected in the degree

of ionospheric variability. But, for a number of reasons, we would not expect sunspot number to be highly correlated with ionospheric personality on a day-to-day basis, and certainly not on an intra-day basis. For one reason, the construction of R is based upon a spatial average over the entire solar disk, and this averaging process has a tendency to eliminate very short-term variations of R . Secondly, there is no physical basis for asserting a direct relationship between sunspot number and ionospheric response. If the same question is asked about solar flares, coronal holes, coronal mass ejections, etc, the answer would be different, with the proviso that time lags be considered in some cases.

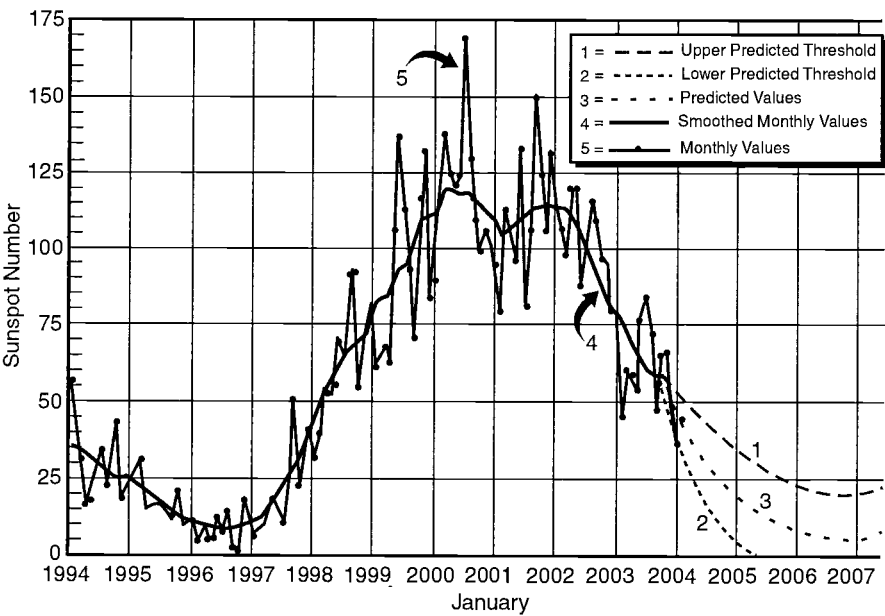


Figure 2-9: Sunspot number variation for solar cycle 23. Monthly averages and smoothed monthly values are given. The dotted lines near the end of the cycle are the upper, median, and lower limits. Data were provided by NOAA-SEC and ISES.

Table 2-4: Sunspot Number Variability

Filter Time Constant	Approximate Sunspot Number Range
11-years	50-100
1-Year	5-150
1-Month	2-175
1-Day	0-350

HF propagation prediction programs in use today all rely on some baseline value of sunspot number (or its proxy), and it is presumed that a running 12-month average of R_z or R_i is to be used as a driver to yield monthly median values of ionospheric parameters (such as f_oF2) as an intermediate product. This is consistent with the fact that the ionospheric data used to formulate almost all climatological models in use today are based upon an evaluation of monthly medians as parameterized by values of SSN, suitably averaged over a 12-month interval. This construction is quite useful for hindcasting, but not as useful for accurate forecasting. Workers have attempted to use monthly or even daily values of the sunspot number. One should be cautious with such approaches, given the inferences of Table 2-4, and the fact that the database indicates that the sunspot number should be entered is the prescribed way for optimization (i.e., 12-month average centered at the time in question). But many HF practitioners have thrown caution to the winds, and have used monthly values without noticeably poor results. On the other hand, use of daily values is a virtual disaster. In fact, it has been shown that an effective sunspot number formed by taking the average over the last five days can strike a good balance between the chaotic behavior of daily values and the damping effect associated with long-term smoothing. Other workers use trend lines or persistence to estimate the sunspot number.

HF prediction models are not the only examples where sunspot number drivers are used in some fashion. TEC and scintillation models also require some sunspot number representation as a driver. We will discuss prediction models in Chapter 5.

An intermediate-term component of sunspot variability can be found by observing the sun through a hypothetical filter having a time constant of several days. The predominant periodicity to be disclosed in this manner is correlated with the solar rotation period, but is significant only if a distinct (longitudinally-isolated) solar active region with a lifetime ≥ 27 days exists. If the lifetime is much smaller than the solar rotation period, then recurrence is impossible. Also, if multiple active regions are distributed over the solar disk, then recurrence phenomena can be smeared out or distended, even if the individual active regions are long-lived. Recurrence, when observed, can be used to predict future effects on the ionosphere and telecommunications performance. We have already seen from Figure 2-5 that the long-term trends in solar and magnetic activity are correlated. The coronal hole example in Figure 2-6 illustrates multiple 27-day recurrences, with an obvious forecasting potential.

There is a greater likelihood that active regions will be isolated at solar minimum than at solar maximum. Nevertheless, if an especially active longitude is persistent, it may still introduce a resolvable 27-day modulation

in solar activity even when the average levels are high. This situation was quite evident during a period in 1990, where solar activity is characterized by the observed 10.7 cm solar flux. From Figure 2-10, we note a steady background level of 150 solar flux units, and a 27-day oscillatory component of ± 40 flux units.

We have already mentioned that the 27-day recurrence of active regions on the sun might provide a basis for updates of the predictions of geophysical disturbances, which are otherwise based upon long-term trends, or climatology. Persistence of features on the sun coupled with solar rotation creates the potential for determination of the geoeffectiveness of coronal holes and resultant solar wind speed changes. Sheeley and his colleagues at NRL [Sheeley et al., 1976, 1978; Bohlin, 1977] have suggested that coronal holes can be long-lived phenomena and should allow predictions of increased solar wind speed to be made for \sim six months in advance. The prediction of solar wind speed, along with an understanding of the interplanetary magnetic field, is quite important in the growth of geomagnetic substorms, and ultimately ionospheric storms. Figure 2-11 shows a very good correlation between the appearance of coronal holes, solar wind velocity, and magnetic disturbance.

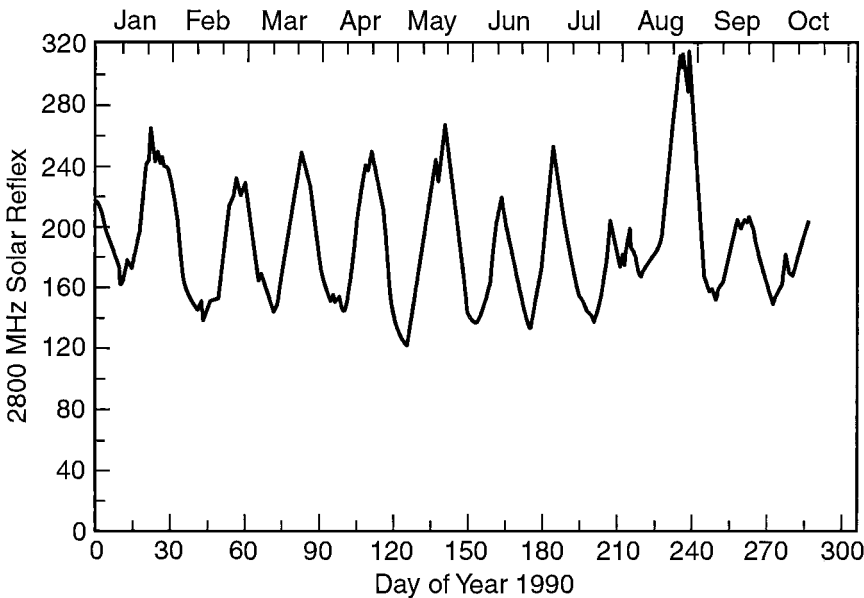


Figure 2-10: Variation of the 2800 MHz solar flux during 1990 showing evidence of a 27-day recurrence in solar activity. Raw data were obtained from NOAA-SEC, Boulder Colorado.

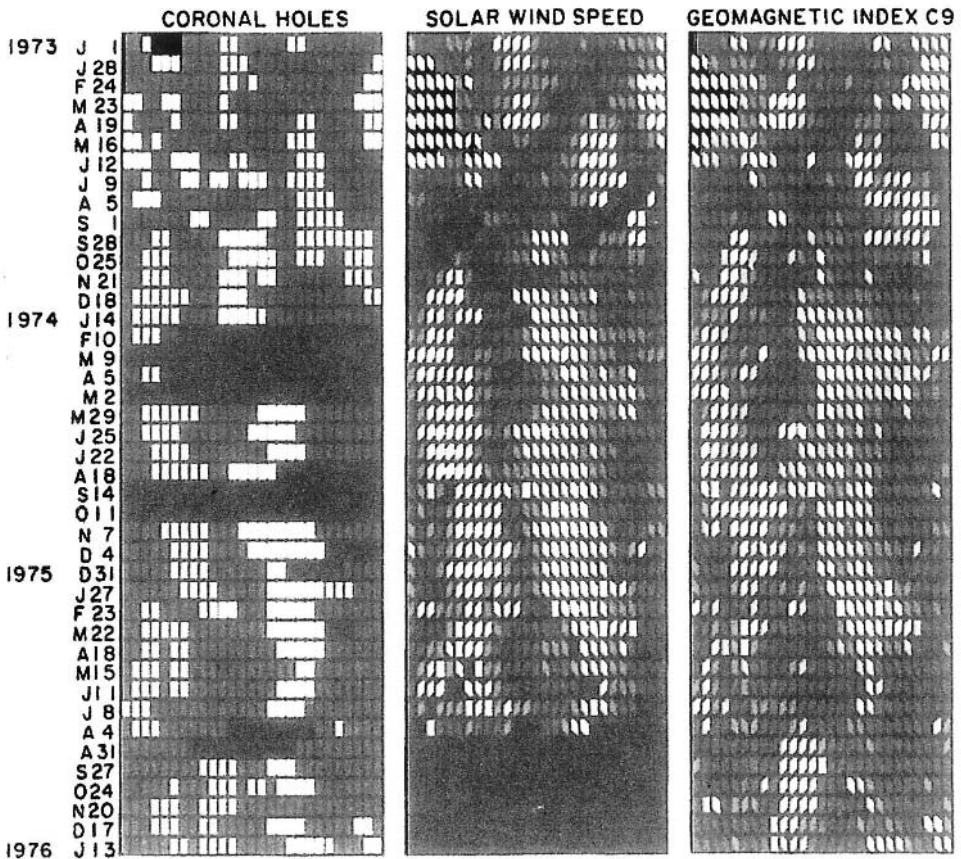


Figure 2-11: A comparison of coronal holes with solar wind speed and magnetic activity. This comparison was made by Sheeley et al. [1976], where the data is arranged in 27-day sequences to correspond to earth rotations.

2.2.7 Solar Flares

One of the more well-known solar events responsible telecommunication disturbances is the solar flare. This is certainly true for HF communications. These events trigger many of the short duration ionospheric events called Sudden Ionospheric Disturbances (SID), and are closely related to other solar phenomena. Sunspot occurrence is closely associated with the observation of solar flares. In general the number of flares observed per solar rotation N_F is proportional to the sunspot number.

$$NF = a(R - 10) \quad (2.6)$$

where R is the smoothed sunspot number over a 27-day rotation period, and a is a constant which ranges between 1.5 and 2. Thus for $R = 110$ (near solar maximum), the value for NF is about 200. This implies that 7 flares/day will be observed on a global basis.

Flares have been classified in terms of the solar surface area that is enclosed as observed in the hydrogen- α line of the solar spectrum. Subflares cover $\sim \leq 2$ square degrees but the largest class of flares may cover about ~ 25 square degrees of the solar surface.

Another optical designation provides a qualitative indication of the brightness of the flare: F=faint; N=normal; B=bright. The most important flare classification for association with ionospheric effects is the flare strength as measured in the x-ray band. Table 2-5 shows the x-ray classifications in the 1-8 Angstrom band. This is a useful scale; in general only those flares with M and X classifications have any practical significance (i.e., enhanced electron production in the D-layer) leading to radiowave absorption. The process of D-layer absorption is covered in Chapter 4.

Table 2-5: Classification of x ray flares

Class of Flare	X-Ray Energy Output E at Earth (Watt/m ²)
X	$E > 10^{-4}$
M	$10^{-5} < E < 10^{-4}$
C	$10^{-6} < E < 10^{-5}$
B	$E < 10^{-6}$

An important illustration of the relationship between the sunspot number, ionospheric storms, and sudden ionospheric disturbances (SIDs) is given in Figure 2-12. The SIDs are directly related to x-ray flares, and the ionospheric storm variation is directly proportional to the incidence of magnetic storm activity. It is evident from Figure 2-12 that SIDs tend to favor the ascending phase of sunspot activity, whereas ionospheric storms favor the descending phase (see Section 2.2.8).

2.2.8 Storms and Declining Solar Activity

Figure 2-12, corresponding to solar cycle 19, suggests that ionospheric storms have a peak following the maximum in sunspot number. This is evidently a general statement. Still, to this day, the popular view within the public at-large, as well as some otherwise well-informed

telecommunication specialists, is that the sunspot maximum period is all important. The myth that the peak of the smoothed sunspot cycle is the only thing that matters was surely broken in the latter half of 2003, a period of decline in sunspot levels. From Figure 2-9 it is seen that there are two minor peaks in the number of sunspots in July and October-November of 2003 but the 12-month running mean is ~ 60 during the period. The period between mid-October and mid-November of 2003 produced some of the most intense flares and stormy periods seen during the entire solar cycle. Figure 2-13 shows the flare production from active region 486 between 10-24-04 and 11-04-04.

Figure 2-14 is a redrawn version of a white light image of the sun on 28 October 2003. The sunspot regions shown 484, 486, 487, 488, and 492 with region 486 being the most important. It was the largest sunspot region observed since 1990, and it retained its size and complex magnetic structure for the full transit across the visible solar surface. There were 17 major flares from October 19th to November 5th, 2003; and 12 originated from region 486.

The magnetic storm phenomenon is probably the most important ramification of sunspot activity. We will now take an abbreviated look at the magnetosphere and geomagnetic storm activity.

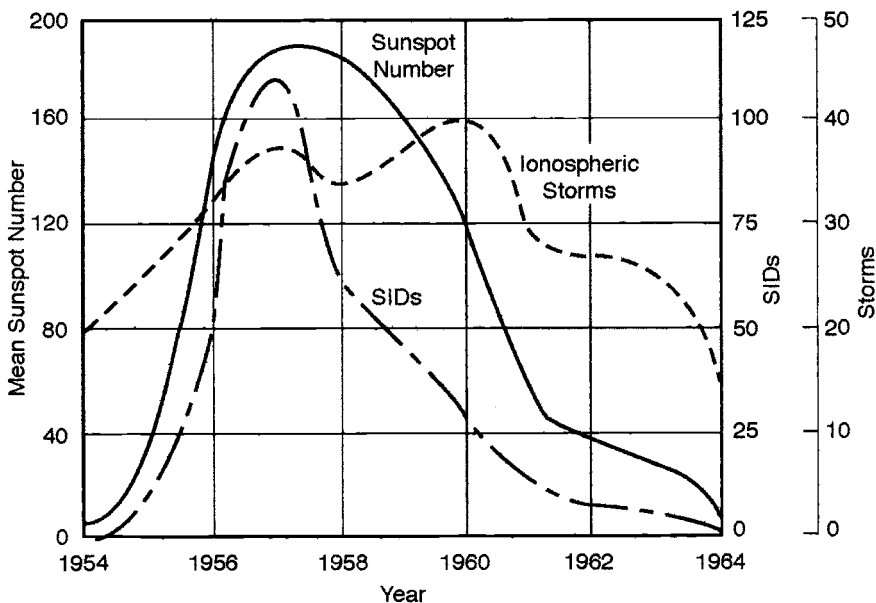


Figure 2-12: Comparison of sunspot number, the number of ionosphere, and the number of SIDs during solar cycle 19 (1954-1964). After Jacobs and Cohen [1979].

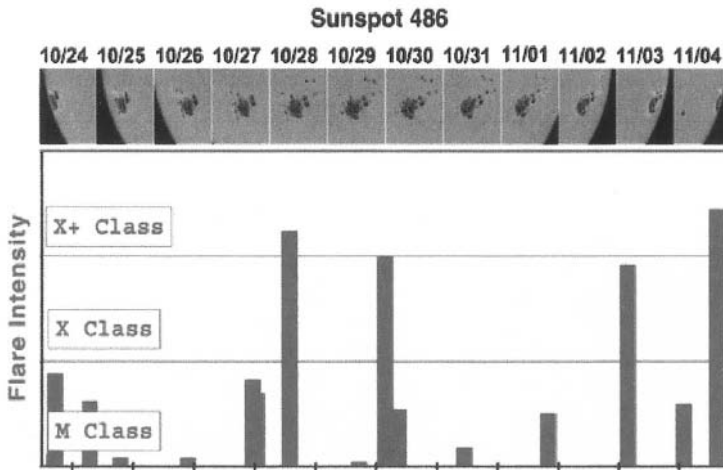


Figure 2-13: Progression of Active Region 486 during the period from 10-24-04 and 11-04-04. The figure is from Simpson [2003]. The image is due to the NASA-SOHO program, the flare data is derived from NOAA, and the compilation is by Metatech Corporation.

Below we have provided a combined excerpt of NOAA-SEC Advisory Outlook #03-44 and Space Weather Advisory Bulletin #03-5.

Summary for October 27-November 4, 2003:

Space weather during the past week reached extreme levels. The dynamic solar region, NOAA Active region 486, continues to produce high levels of solar activity. Region 486 produced a category R4 (severe) radio blackout on October 28 at 11:10 UTC. Associated with this flare was a category S4 (severe) solar radiation storm beginning at 0025 UTC on 29 October. A coronal mass ejection (CME) was also associated, and it produced a G5 (extreme) geomagnetic storm starting at 0613 UTC on 29 October. This persisted at the G3-G5 levels for 24 hours. Region 486 continued to produce solar activity with yet another major flare at 2049 UTC on 29 October, resulting in an R4 (severe) radio blackout. A CME was also associated with this flare. Moving at 5 million miles per hour, the CME impacted the earth's magnetic field at 1620 UTC on October 30th, and produced a category G5 (extreme) magnetic storm. Stormy conditions persisted for 24 hours. Region 486 grew to become the largest sunspot region of cycle 23.

Giant sunspot region 486 unleashed another intense solar flare on November 4th at 1950 UTC. The blast saturated sensors onboard GOES satellites. The last time that happened, in April 2001 (i.e., near the peak of the cycle), the flare that saturated the sensors was classified as an X20, the

biggest ever recorded at that time. The November 4th flare appears to have been stronger. Because sunspot region 486 was near the sun's western limb, the blast was not directed toward earth.

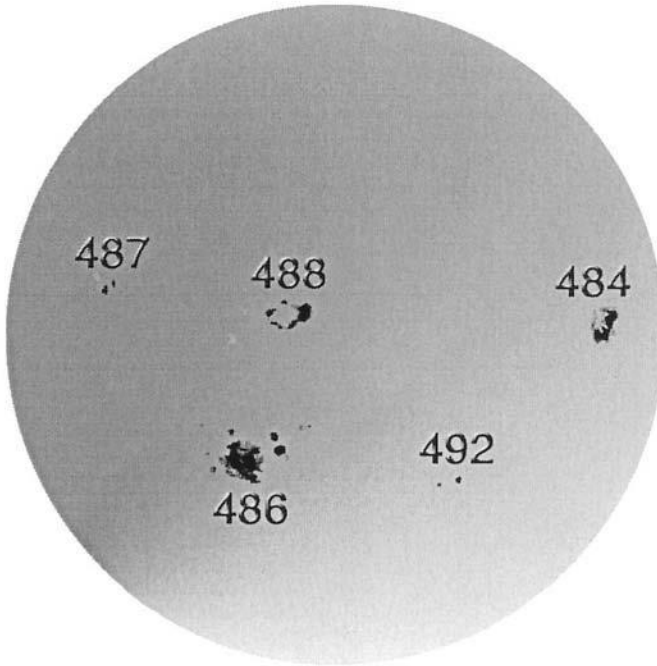


Figure 2-14: Redrawn version of a white light image of the sun on 28 October 2003. This image shows 5 sunspot regions, with Region 486 being the most distinctive. (From EOS, Transactions AGU, Vol.85, No.11, March 16, 2004; the original photograph is courtesy the Solar and Heliospheric Observatory website.)

2.3 MAGNETOSPHERE AND GEOMAGNETIC STORMS

We next turn our attention to the magnetosphere and, in particular, to the coupling of the solar wind, the magnetosphere, and the ionosphere. Much is unknown about these coupling processes, but ongoing studies and campaigns will improve our understanding. We will identify the factors that appear most important, and especially those thought to have a significant bearing on telecommunication systems.

2.3.1 The Geomagnetic Field

To obtain an understanding of the magnetosphere, we must first examine the geomagnetic field. The earth's magnetic field is an important feature since it generally prevents a direct encounter between the ionosphere and energetic particles of solar origin, and especially solar wind. Mars, for example, does not have a magnetosphere, and it is widely held that solar wind "erosion" has eliminated a good portion of the Martian atmosphere. A geographically localized region that does not afford this protection is found in the neighborhood of the magnetic pole. Since the geomagnetic field is an efficient deflector of the solar wind, why are parameters of the solar wind significant in the morphology of the magnetosphere and the ionosphere beneath it?

The magnetic field of the earth resembles a bar magnetic in many respects. The longitudinal field lines are aligned with the axis of a hypothetical magnet at the ends (poles), and the transverse field lines define an equatorial plane that bisects the magnet. If the field around this bar magnetic were to represent the first-order field of the earth, then we see that the polar field line orientation is nearly vertical while the equatorial field lines are horizontal. This is a good model but there are some differences. First, the geomagnetic field is not purely dipolar, and secondly, the axis of the best-fit dipole does not correspond precisely to the rotational axis of the earth. The geomagnetic field is generated by several sources and current systems located within the earth, the ionosphere, and the magnetosphere. The internal sources include a field produced by currents flowing near the earth's core at a depth of about 3000 km. This component dominates all other sources below about five earth radii. The geomagnetic field may be adequately represented by a magnetic dipole tilted with respect to the earth's rotational axis. Some local anomalies result from direct magnetization of crustal material, but these are generally averaged-out at ionospheric heights. The effects of ionospheric/magnetospheric current system sources depend upon the heights being analyzed, but these components are usually small below a few earth radii.

The simplest approximation to the geomagnetic field is an earth-centered dipole directed southward and inclined at about 11.5 degrees to the earth's rotational axis. Thus the North Pole is 78.5°N, 291°E, and the South pole is 78.5°S, 111°E. This model can be improved by displacing the dipole a distance equal to $0.0685 R_e$ toward 15.6° N and 150.9°E, where R_e is the earth radius. This modification places the North Pole at 81°N, 84.7°W, and the South Pole at 75°S, 120.4°E. However, there is considerable wander in the precise coordinate placement if the model is slightly changed because of

longitude sensitivity at high latitudes. There are also secular variations of the field associated with gradual reduction in the dipole field strength, a migration of regional anomalies, a northward movement of the dipole, and other variations. Some approximation methods have been based upon the fact that the geomagnetic field decreases in intensity with the inverse cube of geocentric distance, and these methods extrapolate surface values to ionospheric heights. Such approximations tend to emphasize local effects, but the availability of surface magnetic field properties makes the use of such approaches very tempting. Maps of surface values of the total magnetic field, the azimuthal variation of the compass (declination), and the inclination of the magnetic field from the horizontal (dip) may be found in a number of sources. Figure 2-15 shows the conventions associated with measurements of the geomagnetic field. Units vary depending upon application. The primary transformations are given in Table 2-6.

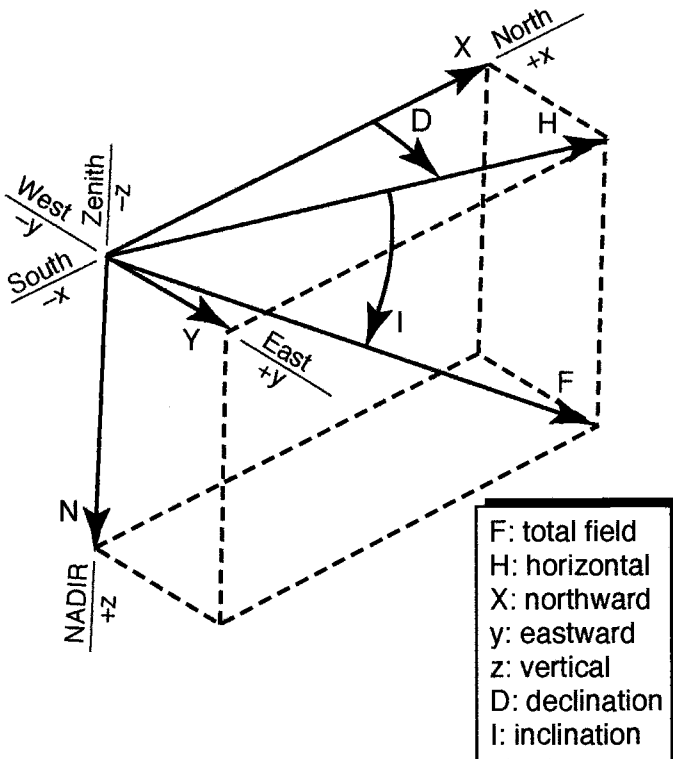


Figure 2-15: Conventions used in Geomagnetic Field Measurements

Table 2-6: Magnetic Field Units and Conversions

Magnetic Induction (B)	1 gamma = 10^{-5} Gauss = 10^{-9} Tesla = 1 nanoTesla
Magnetic Intensity (H)	1 gamma = 10^{-5} Oersted [cgs units] 1 gamma = $10^{-2} (4\pi)^{-1}$ ampere turns/meter [mks units]

The gamma unit (i.e., γ) is employed in some of the older literature, but it is equivalent to the nanoTesla unit (i.e., nT or 10^{-9} Tesla). Table 2-7 is a listing of various field amplitudes of interest.

Table 2-7: Amplitudes of Selected Magnetic Fields

Earth Surface	$\sim \frac{1}{2}$ Gauss	5×10^4 nT
Benign Solar Field	~ 1.0 Gauss	10^5 nT
Disturbed Solar Field	$\sim 10^4$ Gauss	10^9 nT
Solar Wind		~ 6 nT
Secular Field Decay at the Equator		~ 16 nT/yr
Sq Field Variations from Equatorial Currents		0-50 nT
Lunar-Solar Tidal Variations		~ 3 nT
Geomagnetic Storms at Mid-Latitudes (Kp=9)		$\sim 10^3$ nT

There are a number of representations of the geomagnetic field. A description of the methods is given by Knecht and Shuman [1985]. One of the methods that is most physically attractive for demonstrating ionospheric-magnetospheric interactions is one for which the field is modeled in a so-called B - L coordinate frame (see Fig. 2-16). In this system, the field may be exhibited in curves of constant magnetic field intensity B and curves of constant L . In the B - L system, a particular magnetic shell is characterized by a unique L value corresponding to the normalized geocentric distance of the field Vector over the equator. Thus, $L = 2$ corresponds to a field line that reaches its maximum height over the geomagnetic equator at $2 R_e$, where R_e is the earth radius and a convenient normalization factor. This system is quite useful in the study of particles trapped in the magnetosphere such as those found in the Van Allen radiation belts. The terrestrial footprint of a specified field line will occur at two points. These are called conjugate points.

Ionospheric plasma disturbances and resultant telecommunication phenomena are best characterized in terms of geomagnetic rather than geographic coordinates. Accordingly, emphasis should be given to the specification of geomagnetic coordinates for telecommunication terminals, for purposes of space weather assessment.

The dipole method leads to a coordinate system of Geomagnetic Latitudes and Longitudes (i.e., the Geomagnetic Coordinate System). Figure 2-16 depicts a family of Geomagnetic Latitude lines on a Geographic coordinate grid. It is based upon the 1965 IGRF (i.e., International Geomagnetic Reference Field). Other methods include those that replace Geomagnetic Latitude with either Dip Latitude or Invariant Latitude [Jensen et al., 1960]. The Corrected Geomagnetic Coordinate System (CGCS) is a refinement of the Geomagnetic Coordinate system, and like the B-L system, is useful in studies of conjugate effects and other high latitude phenomena.

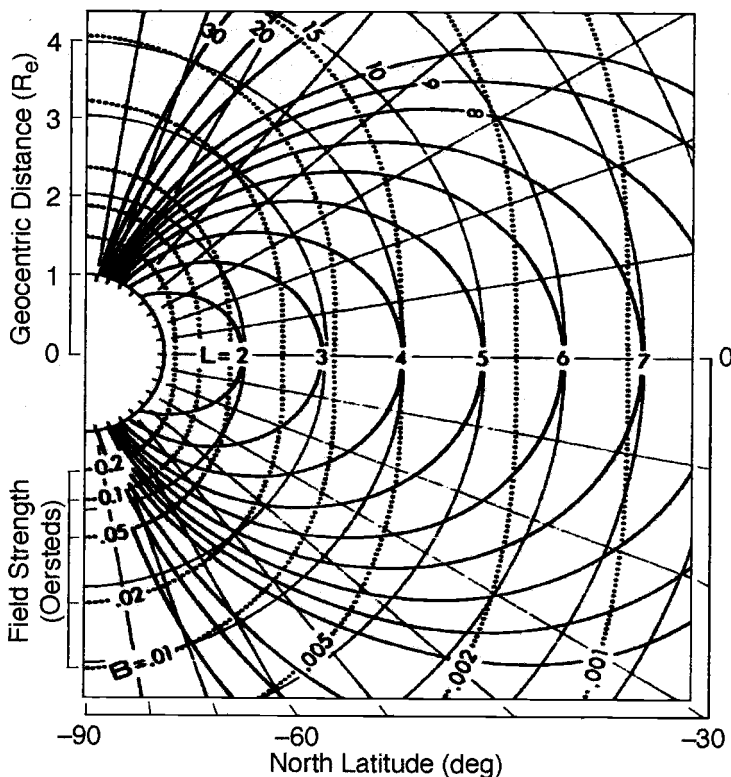


Figure 2-16: The B-L Coordinate System. The curves depicted are in the magnetic meridian plane. The L parameter is related to the height of the field line over the magnetic equator. B is the magnetic field intensity in Oersteds. From Jursa [1985].

Current Methodology uses a representation of the field in terms of a multipole expansion of the magnetic scalar potential function in which the coefficients are based upon a least squares approach to provide a best fit to the field data. This method is now well established and the model, and coefficients, for computing the field are widely available. The internationally

accepted model of the geomagnetic field is the IGRF (mentioned above) with the 1985 version being the most accurate. Previous models have been developed at 5-year intervals beginning in 1965. Coefficients for these models are available from the World Data Center A for Rockets and Satellites at Beltsville, Maryland.

From Figure 2-17, we see that the geomagnetic latitude lines are shifted equatorward in the American sector, relative to Europe and Asia. Knecht and Shuman [1985] have portrayed this situation in a way that gets your attention. They have plotted identifiable land masses in a mercator format, but use Geomagnetic Coordinates for registration (see Figure 2-18).

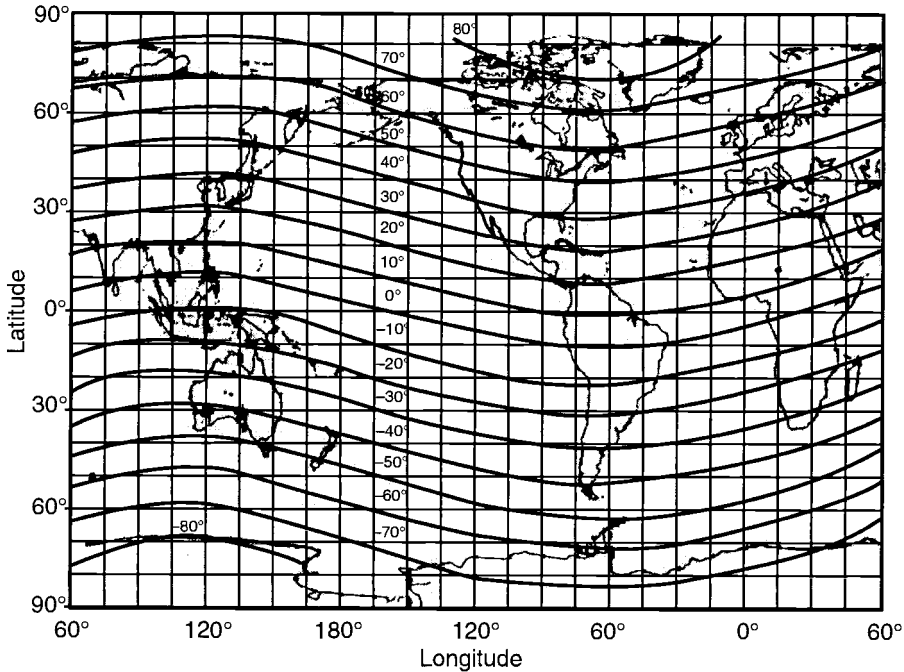


Figure 2-17: Geomagnetic Latitudes (From CCIR [1980]).

Another useful coordinate is the Magnetic Latitude, as opposed to Geomagnetic Latitude. This might be more properly called the Dip Latitude since it is based upon a transformation of observed dip angles by the following formula:

$$\tan \Theta = 0.5 \tan I \quad (2.7)$$

where Θ is the Magnetic Latitude and I is the Dip angle.

are not insignificant within the ionosphere, and since this may restrict geomagnetic control of plasma motion, we do not regard the ionosphere as part of the magnetosphere. Moreover, since the geomagnetic field vanishes beyond the magnetopause, to be replaced by the Interplanetary Magnetic Field or IMF, the magnetosheath is actually not part of the magnetosphere either.

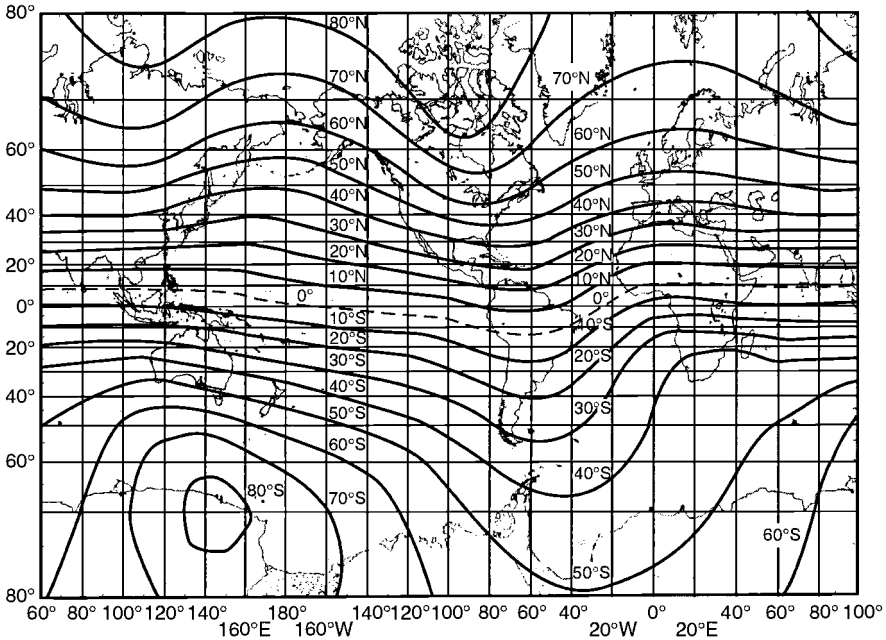


Figure 2-19: Magnetic Latitudes. The dashed line is the Dip equator. This is where the magnetic field is horizontal to the earth's surface. From Valley [1965]

Solar wind particles are typically denied entry to the ionosphere because of the geomagnetic field interaction just mentioned. However, there are some exceptions. Particles may gain entrance through the polar cusp regions. During energetic particle events, this process is enhanced and polar cap absorption (PCA) is the result. Also, because of magnetic merging of the IMF with the geomagnetic field, magnetosheath plasma may be temporarily captured by the plasma sheet (see Figure 2-20).

Another region of interest is the plasmasphere, which serves as a reservoir for ionospheric replenishment during the night and acts as a sink for electrons during the daytime. A very important property of the plasmasphere is its closed field lines. The plasmasphere contains the Van Allen radiation belts. The poleward boundary of the plasmasphere (called the plasmopause)

maps into an ionospheric region called the high latitude trough. Electron concentrations are relaxed in this region. Poleward of the plasmapause, the geomagnetic field lines are no longer closed, but are stretched out well into the magnetotail. This region of open field lines is called the plasma sheet and it has important implications for telecommunication systems at high latitudes. Disturbances within the plasma sheet produce enhanced auroral activity.

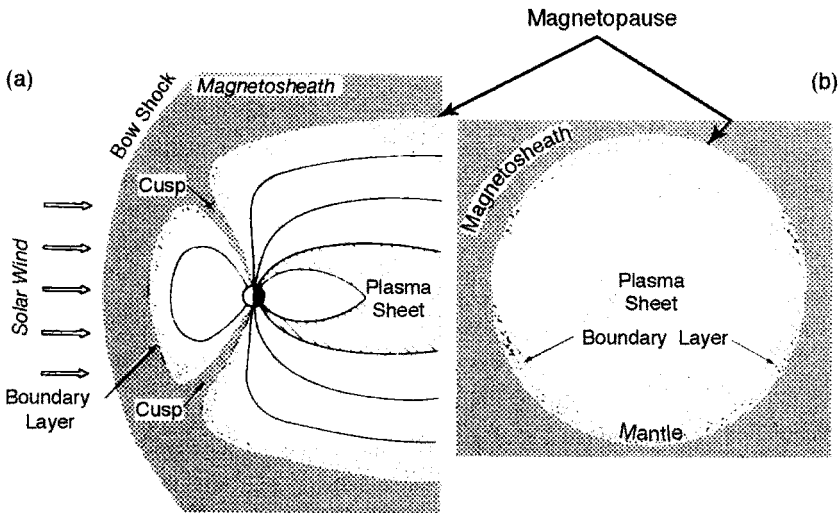


Figure 2-20: A depiction of the magnetospheric regions. From Hill and Wolf [1977].

2.3.3 Geomagnetic Activity Indices

Indices are useful for empirical modeling as well as for forecasting because they provide a convenient parameter set that may be used for driving the model. We have seen that sunspot number R_{12} or the flux index ϕ_{12} are convenient, if not totally representative, of solar activity. The magnetic activity also lends itself to the development of a wide range of index representations. Moreover, the magnetic activity indices are organized and smoothed in a variety of ways that may have the potential for confusing the user who is not an ionospheric specialist. Mayaud [1980] has discussed the array of indices in his book, *Derivation, Meaning, and Use of Geomagnetic Indices*. He traces the history of magnetic index development from the earliest forms to those of the present. Table 2-8 is a list of the current indices

sanctioned by the International Association of Geomagnetism and Aeronomy (IAGA).

Table 2-8: Indices of Magnetic Activity

<i>K-index</i>	Three-hourly quasi-logarithmic index. It is a measure of the irregular variations of the horizontal field component at a specified station or group of stations. For example K_{FR} corresponds to the Fredericksburg site, and K_p is associated with the planetary “average” value. The values of K run from 0-9 with “9” representing the most disturbed condition. K_p is derived from 12 stations between geomagnetic latitudes 48-63 degrees.
<i>Dst-index</i>	Hourly Index associated with low latitude magnetic activity. It is designed to be a measure of the ring current in the magnetosphere (i.e., that region above the geomagnetic equator at ~ 5.6 earth radii). <i>Dst</i> stands for “disturbance amplitude storm time”, and its units are nT. Four midlatitude sites are used in the construction of <i>Dst</i> .
<i>AE-index</i>	Auroral electrojet activity index. This is an hourly index derived from a number of auroral stations.
<i>Q-index</i>	High latitude index with a 15-minute time resolution. It is related to the auroral oval position, and is employed in several propagation prediction algorithms (viz., ICEPAC; see Chapter 3). $Q \sim 2K_p - 3.5$ (The relationship used by AFWA Space Weather Operations Center [ref: NWRA website])
<i>A-index</i>	Daily index of magnetic activity at an individual station or a global array of stations. The <i>A-index</i> ranges between 0-400. It is the linear equivalent to K . (See Table 2-9). The three-hourly <i>K-indices</i> may be converted to a set of eight three-hourly <i>A-indices</i> that are averaged to yield a single daily <i>A-index</i> . The U.S. Air Force has developed an operational (planetary) A_p index corresponding to shorter time frames. Such indices can be employed in <i>foF2</i> correction models such as STORM (see Chapters 3 and 4).
<i>aa-index</i>	Three-hourly indices computed from <i>K-indices</i> of two nearly antipodal magnetic observatories with an invariant latitude of ~ 50 degrees. This index is designed to provide an index of global activity.

The most widely used index is K_p . It is used for ionospheric predictions. However, if we want a simple daily average for the magnetic activity, the fact that K_p is quasi-logarithmic makes it a mathematically poor choice. Even so, a number of studies have used the sum of the eight 3-hourly values of K_p to represent the smoothed daily behavior. The *A-index* is a better choice for use in averaging. Table 2-9 gives a transformation between *A-index* and *K-index*.

Magnetic field data may be obtained from publications and bulletins issued by the International Service of Geomagnetic Indices (ISGI) or the International Association of Geomagnetism and Aeronomy (IAGA) by writing the publications office of the International Union of Geophysics and

Geodesy (IUGG) located in Paris, France. The World Data Centers (WDC) also maintain archives of geomagnetic data. Subcenters of WDC-A (USA) are located in Boulder, Colorado (NGDC) and Greenbelt, Maryland (NSSDC). Bulletins issued by NOAA/NGDC are also mailed to interested users, and NOAA-SEC and Regional Warning Centers of ISES publish reports of the various indices. Generally speaking the *K-index* (or its *A* equivalent) is available from the same sources that issue sunspot number reports and advisories.

Table 2-9: Transformation from *K-index* to *A-index*

<i>K-index</i>	<i>A-index</i>
0	0
1	3
2	7
3	15
4	27
5	48
6	80
7	140
8	240
9	400

2.3.5 Real-Time Geomagnetic Data

Magnetometer stations have been established at many locations, and have been quite useful in long-term aeronomic studies as well as in short-term experimental campaigns. A list of stations providing data to the various World Data Centers is given in the compilation by Shea et al. [1984]. Recently attention has been given to a more current assessment of geomagnetic conditions, and the INTERMAGNET program provides near real-time geomagnetic data to Geomagnetic Information Nodes (GINS) for analysis and timely dissemination of data to users [Green, 1990]. The following GIN stations are in operation: Edinburgh, Scotland (British Geological Survey); Golden, Colorado (U.S. Geological Survey); Kyoto, Japan (Kyoto University); Hiraio, Japan (Communications Research Centre); Ottawa, Canada (Geological Survey of Canada); and Paris, France (Institut de Physique du Globe de Paris). The establishment of this network is consistent with the creation of other real-time ionospheric data networks and solar monitoring systems.

2.3.6 Magnetic Storms and the Ionosphere

It is now widely believed that auroral activity is embodied in the auroral substorm concept described by Akasofu [1964], and that the auroral substorm is only one manifestation of a general process called a magnetospheric substorm [Akasofu, 1968, 1977]. The most dramatic consequence of the magnetospheric substorm is the aurora. The nature of magnetic storms has been refined since the late 1970s. Excellent accounts are found in the one of the NATO science series books, *Space Storms and Space Weather Hazards* [Daglis, 2001], and in AGU Geophysical Monogram 98 entitled *Magnetic Storms* [Tsurutani, 1997].

While the solar wind blows smoothly through the magnetosheath, the topology of the magnetosphere is not disturbed. The plasma sheet is calm and auroral displays are subdued as long as this quiet condition exists. When sunspot activity is at high levels the probability for disturbed aurora and geomagnetic storms is increased. Evidently the enhanced solar wind, which arises when sunspot activity, active regions and solar flares are most prevalent, disturbs the magnetospheric boundary as well as the plasma sheet within the magnetotail. More definitively, coronal expansion phenomena, including Coronal Mass Ejections (CMEs) and coronal holes are major sources of high-speed wind streams. Coronal holes can emerge in a transient fashion, but are usually long-lived and can result in recurrent effects (see Figure 2-6). The coronal hole is a solar feature that can occur even during solar minimum conditions. This can explain why ionospheric disturbances are sometimes observed to occur in the absence of any apparent solar activity (as measured in terms of sunspots).

A crude picture of the magnetic substorm process is given in Figure 2-21. An important factor in the generation of substorm energy is the direction of the Interplanetary Magnetic Field (IMF) along the dipole axis of the earth. When it is directed southward, as shown in Figure 2-20, the plasma sheet becomes pinched driving ionization toward the polar regions. Sheeley et al. [1976] associated high speed solar wind and geomagnetic activity (See Figure 2-11). The current view is that solar wind speed and the IMF direction are fundamental discriminants.

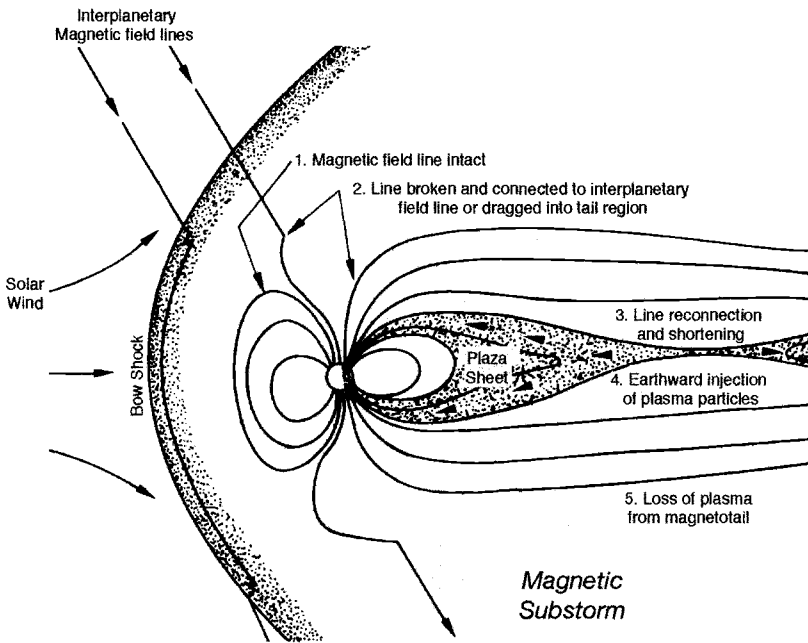


Figure 2-21: Anatomy of a magnetospheric substorm.

The solar wind exhibits fluctuations when high-speed wind streams mix with the ambient solar wind. These fluctuations may be transferred to the N-S component of the IMF. A southward fluctuation may introduce a series of substorms until the excess energy associated with differential merging is exhausted. Differential merging is a process in which the dayside merging rate is in excess of the nightside merging rate. It is a phenomenon that is thought to build up stresses along field lines within the plasma sheet in the tail region. Substorms occur in groups and this process serves to produce a pulsation of the auroral structures. A major geomagnetic storm may be regarded as the integration of a series of substorms. The sequence of events is shown in Figure 2-21.

As the field lines associated with the IMF turn southward, they merge with geomagnetic field lines inside the bow shock region (in the vicinity of the cusp) and flux is transferred from the dayside to the nightside of the magnetosphere. This buildup in potential energy lasts for less than an hour. Subsequently the energy is released as open field lines in the magnetotail become pinched and some of them become reconnected. As the field lines snap into a dipolar configuration, energetic particles are injected toward the earth, forming arcs. These aurorae arcs form beautiful nocturnal displays in regions in the Northern and Southern hemispheres located just poleward of

the midlatitude trough but generally equatorward of the polar cap. These regions were shown by Feldstein to be represented best by ovals anchored at their center by the geomagnetic pole.

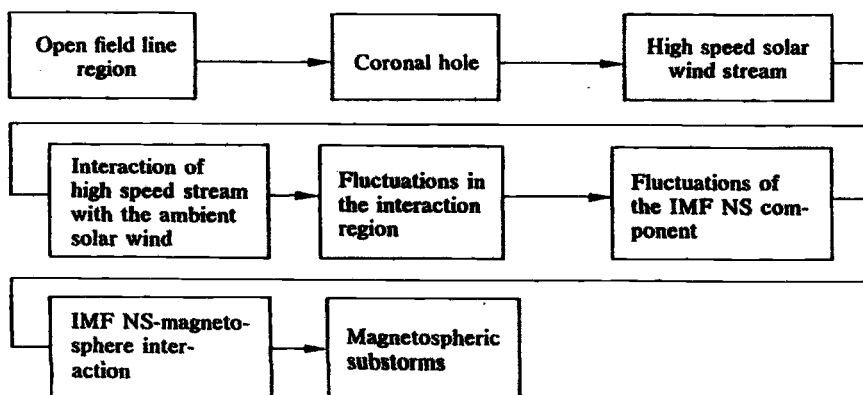


Figure 2-22: Flow Chart of processes leading to the magnetospheric substorm. Working backwards, we see that the conditions for substorm development include (i) a high speed solar wind stream, and (ii) fluctuations of the NS component of the IMF. It has been shown that southward directed B_z is generally a necessary condition. This high-speed stream generally has its origin in the solar corona. Coronal holes (having long-term effects and potential for recurrence) and transient CMEs are possible sources.

Since the auroral oval is a geomagnetic feature, an interesting diurnal pattern emerges because of the departure of geomagnetic from geographic coordinates. Figure 2-23 shows how the steady state auroral oval appears to move as a function of local time. Notice how Iceland becomes alternately an auroral and nonauroral station even though the magnetic activity is assumed to be fixed. This has important consequences for some telecommunication systems. Our understanding of the dynamics of the aurora and its location has been greatly enhanced by the use of optical imagers from the Defense Meteorological Satellite Program (DMSP). But additional resources have been applied over the years. Striking images of the auroral zone have been obtained over the northern and southern hemispheres using several satellites, including: (i) DMSP (from the 1970s), (ii) the Dynamics Explorer Satellite (from the 1980s; see Figure 2-24), and (iii) IMAGE (currently). From Figure 2-24, we see that Greenland and Iceland are both well circumscribed by the outer ring of the auroral oval. Although the oval may expand and contract over time, it is remarkable how consistent this pattern can appear from space. Refer to Figure 1-4 in Chapter 1 for pictures of the oval during the year 2000 Bastille Day storm using the IMAGE satellite. It is noteworthy that the Solar-

Terrestrial Dispatch organization (STD) publishes on its website selected images of the north polar region from NASA’s IMAGE satellite and from the University of Iowa Visible Imaging System (VIS) associated with the POLAR satellite. The company also offers a special product called the STD Auroral Monitor. The STD website is but one example of how the commercial world can use the output from space sensors to offer its customers tailored output. Other companies with web products include Northwest Research Associates, Metatech Corporation, Space Environment Technologies, and Radio Propagation Services. See Chapter 5 for more examples.

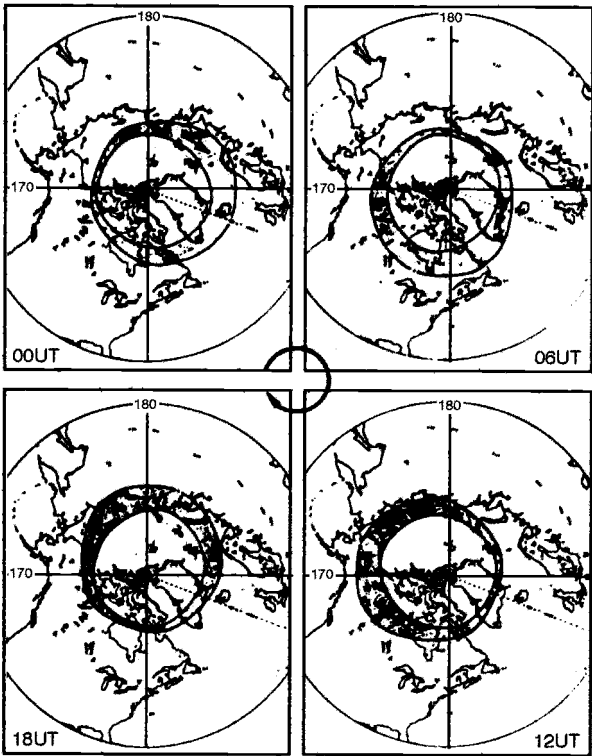


Figure 2-23: The diurnal motion of the auroral oval in geographic coordinates. From Goodman [1991], after Jursa [1985].

Returning to phenomenology, it has been found that the auroral oval thickness increases as the magnetic activity increases and the diameter of the oval expands equatorward. This process is depicted in Figure 2-25. As has been indicated, one of the features of a geomagnetic storm is the equatorward expansion of the auroral oval. Figure 2-26, based upon TIROS observations, shows this characteristic equatorward motion following a period of strong storm activity on November 20-21, 2003. Magnetic activity is highly correlated with the source that drives this motion, and its time history for the period, in terms of the estimated Kp , is depicted in Figure 2-27.

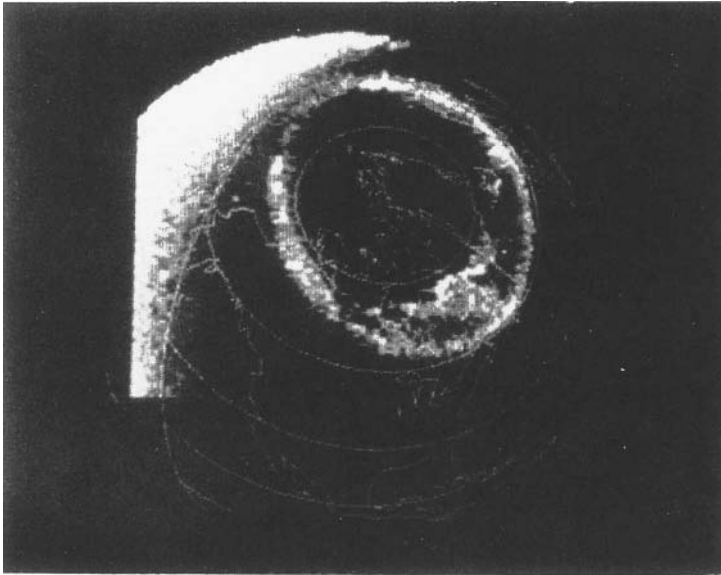


Figure 2-24: Auroral Oval image of North America obtained with the University of Iowa instrumentation aboard the Dynamics Explorer (DE1) on November 8, 1981, a period of intense solar and magnetic activity. From Jursa [1985], after Whalen et al. [1989].

There is a clear lag between the Kp time series and the resulting equatorward movement of the oval. There is also a diminution in the total electron content, TEC (and the parameter $foF2$) at high latitudes as a result of the storm activity. It turns out that the effective sunspot number, $SSNe$, developed by Northwest Research Associates, is crudely proportional to the globally-averaged $foF2$ value. One would expect a global response to be a smoothed-out and somewhat delayed version of the high latitude response. This expectation is consistent with the data in Figure 2-28 that shows the so-called effective sunspot number, $SSNe$, following the same trend in oval

movement, and is delayed in time. The drop in *SSNe* is indicative of a general worldwide diminution in electron concentration. This matter will be discussed further in Chapters 3, 4 and 5.

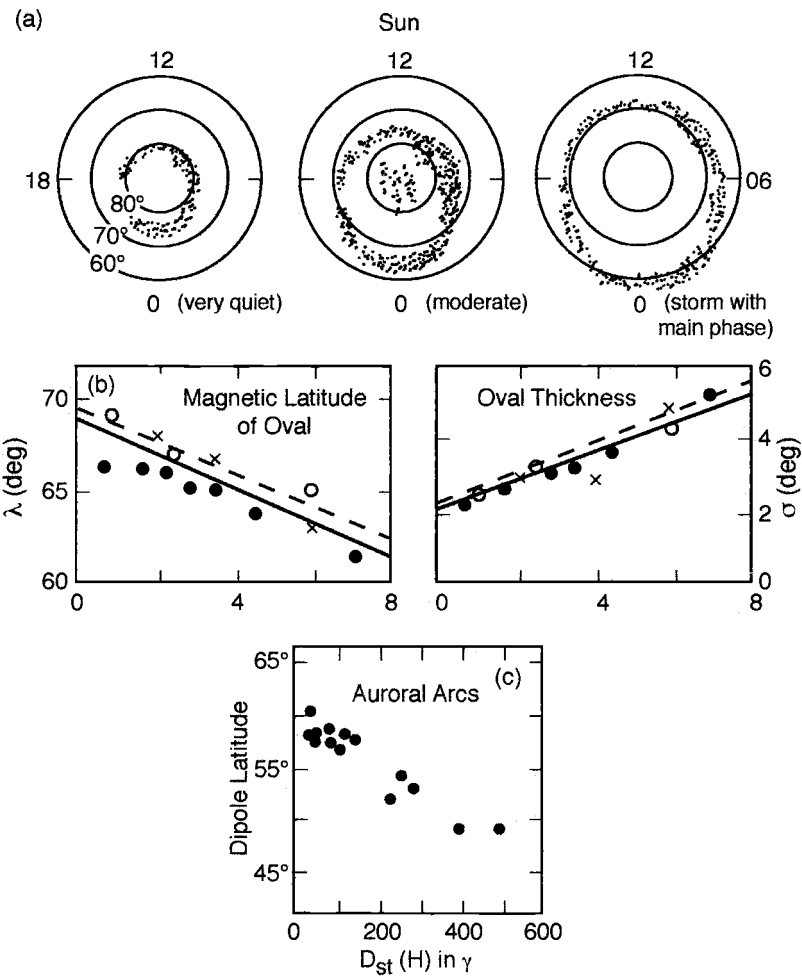


Figure 2-25: (a) Cartoon illustrating the descent of the auroral oval, (b) Median latitude and longitude and oval thickness as a function of *K*-index, (c) Dipole latitude of the oval as a function of the *Dst*-index. Looking at graphs (a), under very quiet conditions, characterized by *Kp* < 3, the auroral oval contracts approaching 70 degrees in the limit. Under disturbed conditions, for which *Kp* > 5, the oval expands approaching 60 degrees in the limit. Equatorward expansion may be larger under strong magnetic storm conditions associated with a main phase. From the depictions (a), we see that the oval is not quite symmetric about the magnetic pole. The nocturnal oval (i.e., anti-sunward side) is more distended equatorward regardless of storm conditions. This is exacerbated in the American sector since the magnetic pole is positioned in northern Canada.

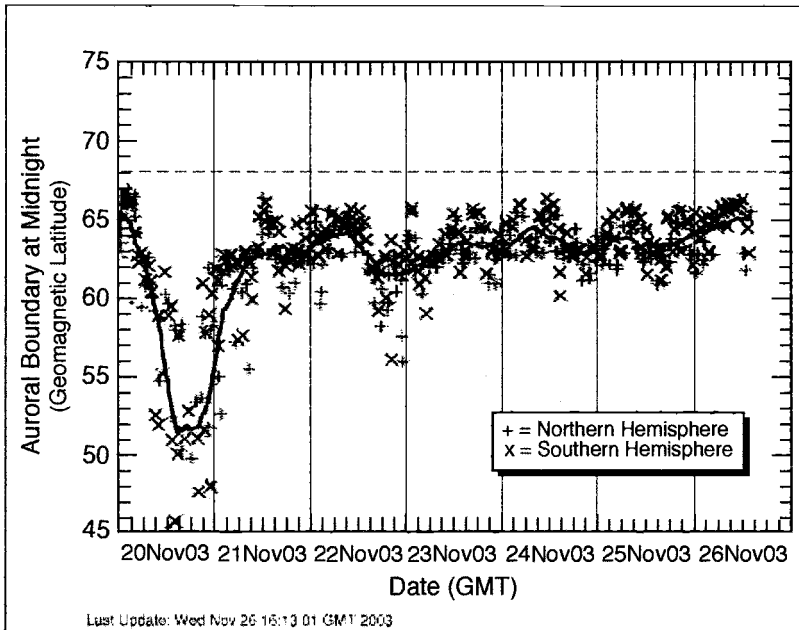


Figure 2-26: The auroral oval boundary position. Graphic courtesy Northwest Research Associates using NOAA-SEC data as input. Refer to Figure 2-27 and Figure 2-28. From NWRA web site, 2004.

A geomagnetic storm develops as the result of the energy transferred from the solar wind to the magnetosphere in a series of substorm events. In macroscopic terms, one may regard the geomagnetic storm as composed of two parts: (i) an initial (short-lived) positive phase associated with an increase in the horizontal component of the magnetic field, which is followed shortly by enhanced auroral displays, and (ii) a main negative phase (or bay) in the horizontal field intensity which may last for several days. The initial phase is associated with short-lived enhancements in electron concentration at ionospheric heights, while the main phase is associated with large-scale diminutions in electron concentration. These effects are often called ionospheric storms to emphasize the ionospheric disturbances involved. It should be noted, however, that the ionospheric response to magnetic storm activity is not always the same. There are differences in latitude, and the effects also depend upon season. More discussion may be found in Chapter 3 where the ionosphere is more fully examined.

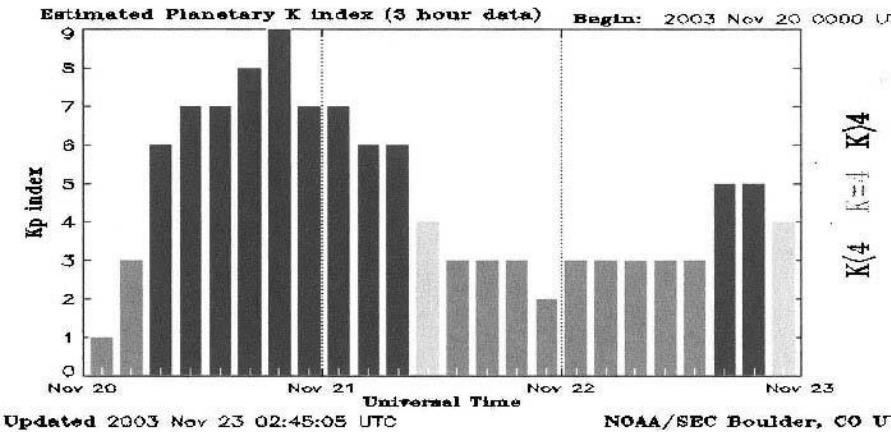


Figure 2-27: Estimated Kp index during the November 20-21 storm. Refer to Figure 2-26 and Figure 2-28. Data provided by NOAA-SEC, Boulder CO.

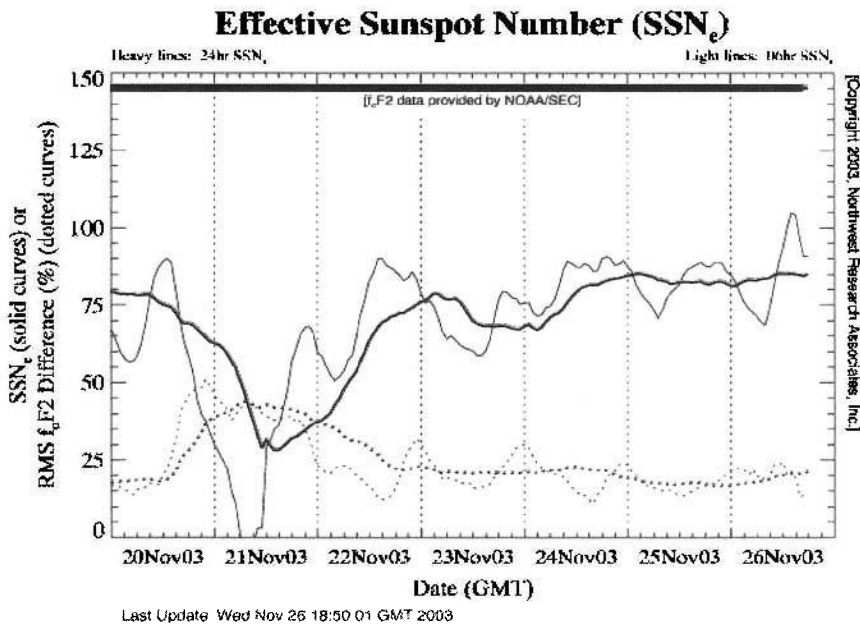


Figure 2-28: Effective Sunspot Number. The effective sunspot number is obtained by matching the tendencies associated with sounder data at selected locations with predictions from a model parameterized by the sunspot number. Graph due to Northwest Research Associates using data from NOAA-SEC sounder database. Refer to Figure 2-26 and Figure 2-27. From NWRA web site, 2004.

2.3.7 The Halloween Storm Period of 2003

As noted in Section 2.2.8, The October 2003 period was an extraordinary period of significant solar activity. Region 486 produced two enormous x-ray flares, with accompanying CMEs, on 28 and 29 October, 2003. The amplitudes of the flares were \sim X17 and \sim X10 respectively as depicted in Figure 2-13. Extreme (i.e., G5) magnetic storms were introduced following impact of both of the CMEs. The second storm has since been termed the Halloween storm in view of its coincidence with the well-known holiday, but its impact on the ionosphere made it noteworthy as well. Figure 2-29 shows the flare activity for the period of interest, and Figure 2-30 shows the magnetic activity response. During these stormy periods, high frequency communications were virtually impossible over uncompensated high latitude paths. The variation in electron concentration was significant for midlatitude sites as well as high latitude sites. We discuss these ionospheric effects in Chapter 3, and some factors related to specific systems in Chapter 4. Indeed, telecommunication performance was degraded for a variety of system types. Ionospheric effects upon the FAA WAAS system are indicated in Chapter 4. The U.S. Department of Commerce (i.e., NOAA, National Weather Service) has published a *Service Assessment* [NOAA-NWS, 2004] detailing the space weather storms of October 19th through November 7th, 2003. Table 2-10 is a chronology of events

Table 2-10: A Summary of Events for the period October 19-November 7, 2003

- October 28, 2003: 1110 UTC: X17 flare from Region 486
- X17 flare produces R4 (severe) radio blackout & solar radio bursts
- X17 flare followed by radiation storm, reaching S3 (strong) levels and S4 (severe) levels after 13 hours
- X17 flare was followed by fast CME. The CME was observed by LASCO on SOHO spacecraft, and had a speed of 2,125 km/sec. The CME reached the earth in 19 hours..
- The X17-related CME impacted the ionosphere and produced a G5 (extreme) geomagnetic storm. This storming lasted 27 hours. This was the 6th most intense storm since 1932.
- October 29: 2049 UTC: X10 flare from Region 486
- X10 flare produces R4 (severe) radio blackout
- X10 flare produces S3 radiation storm
- X10 flare followed by Fast CME with a speed of 1,948 km/sec, reaching the earth in 19 hours. (1600 UTC on October 30, 2003)
- The X10-related CME impacted the earth and introduced a G5 (extreme) geomagnetic storm lasting 24 hours.
- November 4, 2003: 1950 UTC: X28 flare emitted from region 486. This flare occurred near the west limb of the sun, so the impact was minimal. The CME was directed away from the earth. The X28 flare is thought to be the largest since these events have been recorded.

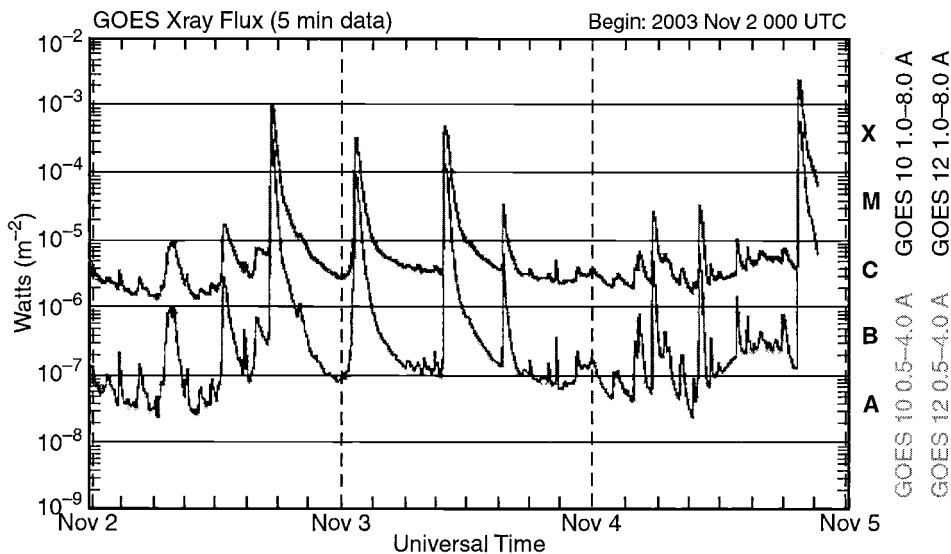


Figure 2-29: GOES X-ray flare activity for the Halloween storm period. Data provided by NOAA-SEC, Dept. of Commerce

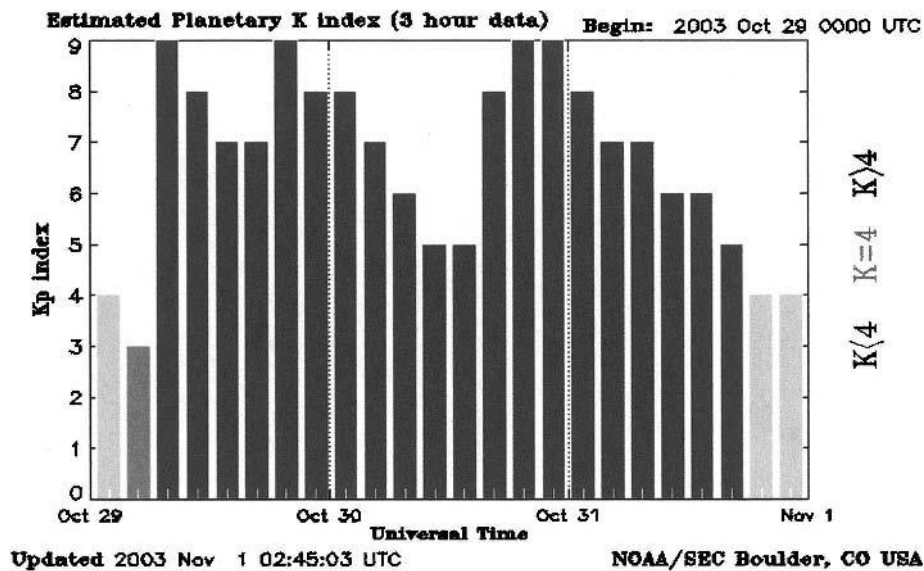


Figure 2-30: Magnetic activity for Halloween storm period. (Data provided by NOAA-SEC, Dept. of Commerce, Boulder CO.)

Given the enormity of the Halloween storm events discussed above, one might say that such isolated situations are sufficient to justify a significant investment in space weather observations and around-the-clock vigilance. But this probably not the case. One has to recognize that such events are not normal occurrences. While they may play havoc, they are rare. From the NOAA assessment report [NOAA-NWS, 2004] a listing of the top 20 radiation storms and the top solar flares have been tabulated. These are given in Tables 2-11 and 2-12. Data for solar cycles 21, 22, and 23 are listed. We see that the Top-20 listing includes 3, 9, and 8 radiation events for cycles 21, 22, and 22 respectively. These events may cause PCA events (of importance to HF communication over the poles) and can lead to radiation exposure for passengers and crew for transpolar flights. One radiation storm from the October-November 2003 period appears in Table 2-11. This occurred on October 28, 2003 (rank 4).

The X-ray flare listing in Table 2-12 indicates that the largest flares numbered 4, 10, and 6 for solar cycles 21, 22, and 23 respectively. Flares cause short wave fades (SWFs) for HF systems, but their importance may be greater as an indicator of delayed effects such as radiation storms, PCA events, and geomagnetic storms. There are 3 flares from the October-November 2003 period in Table 2-12: 11-04-2003 (rank 1), 10-28-2003 (rank 4), and 10-29-2003 (rank 20).

Probably the more important listing is that of magnetic storms. In this instance the NOAA Service Assessment [NOAA-NWS, 2004] has provided the Top-30 Geomagnetic storms since 1932 based upon the Potsdam “running” Ap index. It is well known that geomagnetic storms introduce significant ionospheric perturbations of global significance. Table 2-13 indicates that the largest geomagnetic storm was on December 18, 1941 and that two storms during the “Halloween” period of 2003 (i.e., October 29 and October 30) were respectively ranked 6 and 16 on the 1932-2003 list.

Table 2-11: The Greatest Twenty Radiation Storms (GOES proton flux > 10 MeV since 1976)

Rank	Intensity (pfu) $\times 10^3$	Date (mm-dd-yyyy)	Rank	Intensity (pfu) $\times 10^3$	Date (mm-dd-yyyy)
1	43	03-23-1991	11	7.3	11-30-1989
2	40	10-19-1989	12	4.6	05-09-1982
3	31.7	11-04-2001	13	4.5	09-29-1989
4	29.5	10-28-2003	14	3.5	03-08-1989
5	24	07-14-2000	15	3	06-04-1991
6	18.9	11-22-2001	16	2.9	06-11-1982
7	14.8	11-08-2000	17	2.7	10-30-1992
8	12.9	09-24-2001	18	2.52	04-21-2002
9	10	02-20-1994	19	2.5	04-25-1984
10	9.2	08-12-1989	20	2.36	10-01-2001

Table 2-12: Top Twenty Solar Flares**

Rank	X-ray Intensity	Date (mm-dd-yyyy)	Rank	X-ray Intensity	Date (mm-dd-yyyy)
1	X28e	11-04-2003	11	X12	12-15-1982
2	X20e	08-16-1989	12	X12e	06-04-1991
3	X20c	04-02-2001	13	X12e	06-06-1991
4	X17	10-28-2003	14	X12c	06-11-1991
5	X15e	07-11-1978	15	X12c	06-15-1991
6	X15e	03-06-1989	16	X10	12-17-1982
7	X13e	04-24-1984	17	X10	05-20-1984
8	X13c	10-19-1989	18	X10	01-25-1991
9	X12c	06-06-1982	19	X10	06-09-1991
10	X12e	06-01-1991	20	X10	10-29-2003

** NOAA GOES X-Ray instrument, as observed since 1976. The “e” affixed to the X-ray intensity indicates that the value is estimated since the saturation level for the instrument was reached. By 1993, the saturation level was elevated to the X17.4 level.

Table 2-13: The Top-30 Geomagnetic Storms

Rank	Ap Value	Date	Rank	Ap Value	Date
1	312	09-18-1941	16	220	10-30-2003
2	293	11-12-1960	17	216	07-08-1958
3	285	03-13-1989	18	215	03-28-1946
4	277	03-23-1940	19	214	09-22-1946
5	258	10-04-1960	20	212	03-01-1941
6	252	10-29-2003	21	212	07-26-1946
7	252	07-15-1959	22	203	08-19-1950
8	251	03-31-1960	23	201	09-04-1982
9	241	05-25-1967	24	199	02-07-1946
10	229	07-11-1982	25	199	02-11-1958
11	228	02-07-1986	26	196	05-12-1949
12	226	03-29-1940	26	196	06-04-1991
13	223	08-04-1972	28	195	03-24-1946
14	222	07-05-1941	29	193	05-09-1992
15	221	09-02-1957	30	192	07-14-2000

2.4 MOTIVATION FOR SPACE WEATHER OBSERVATIONS

In this chapter we have examined the nature of solar activity, and have stipulated that a host of events on the sun can give rise to perturbations in the earth’s magnetosphere and ionosphere. Electromagnetic radiation does not interact with the geomagnetic field, but X-ray flares can introduce photoionization of atmospheric species. This leads to radiowave absorption in

the lower ionosphere on the sunlit side of the earth. The explosive expulsion of solar cosmic rays (i.e., protons), being deflected toward the polar region, can introduce long-lived radiowave absorption events (i.e., PCA) within the polar cap, and may also introduce radiation hazards for aviation executing transpolar flight plans. While solar flares are a known source of performance impairment for telecommunication systems, the effect of high-energy protons (i.e., solar cosmic rays) and earth-directed coronal plasma (viz., enhanced solar wind and CMEs) are even more important.

For X-ray flares, the impact is virtually immediate; hence the telecommunication system could be designed to compensate by “brute force” rather than through application of diversity techniques. For example, to counter strong power-robbing absorption without trying to play “catch-up”, the system should have adequate “margin” incorporated within the design. Often this is too costly. In practice, some systems simply “ride” out the flare effect, which may last less than an hour in most instances, even at HF.

The good news for the non-electromagnetic sources, like CMEs, is that some lead-time is possible for more efficient exploitation by adaptive systems. Moreover the effects usually last awhile. Thus any changes made in system parameters or operational procedures will not have to be undone shortly after making the original change. What a system manager does not want is a situation in which an adaptive subsystem is constantly required to change its operational state. In such a situation, the system spends too much of its time adjusting to the environment, and too little time fulfilling its mission. The overhead required to “chase-down” the telecommunication environment can be too large. This suggests that multiple events that are superimposed can play havoc.

The lesson to be taken from this summary statement is that a timely analysis of solar phenomena can be critical to the successful operation of some telecommunication systems. At the very least, solar observational data sets are critical in forecasting the level of magnetic activity for some time in the future. Having this data might enable an estimation of ionospheric parameter variations from several hours to days in advance.

Table 2-14 is a listing of the solar sources of space weather that have the potential to impair certain classes of telecommunications systems. The ionospheric effects are discussed in Chapter 3 and the system effects are covered in Chapter 4. Forecasting can be used as a countermeasure for systems that are operationally agile or quasi-adaptive in nature. Forecasting systems and real-time data sources are discussed in Chapter 5.

Table 2-14: Solar Sources of Telecommunication System Impairment

Source
Coronal hole
Coronal Mass Ejection (CME)
Energetic Particle (i.e., proton) event
Solar flare
Solar radio burst

- - -

2.5 REFERENCES

Akasofu, S.I., 1964, "The Development of the Auroral Substorm", *Planetary Space Science*, 12:273.

Akasofu, S.I., 1968, *Polar and Magnetospheric Substorms*, D. Reidel Publishing Co., Dordrecht, Holland.

Akasofu, S.I., 1977, *Physics of Magnetospheric Substorms*, D. Reidel Publishing Co., Boston.

Bohlin, J.D., 1977, "Extreme Ultraviolet Observations of Coronal Holes. 1. Locations, Sizes, and Evolution of Coronal Holes, June 73-Jan 84", *Solar Physics* 51:377-398.

CCIR, 1980, "CCIR Atlas of Ionospheric Characteristics", Supplement No.3 to Report 340, (based upon CCIR Meeting Kyoto, 1978), ITU, Geneva; p.29.

Chapman, S., 1968, *Solar Plasma, Geomagnetism and Aurora*, Gordon and Breach, New York, London and Paris, p.28-32 (references have been made specifically to Figs.1.11 and 1.12 in Chapman's text).

Daglis, I.A. (editor), 2000, *Space Storms and Space Weather Hazards*, NATO Science Series, Physics and Chemistry, Volume 38, Kluwer Academic Publishers, Dordrecht, Boston, and London, 2000.

Friedman, H, 1985, *Sun and Earth*, Scientific American Books, New York.

Gibson, E.G., 1973, "The Quiet Sun", NASA SP-303, National Aeronautics and Space Administration, USGPO, Washington, DC.

Goodman, John M., 1991, *HF Communication: Science and Technology*, Van Nostrand Reinhold, New York (out-of-print; now available through JMG Associates, 8310 Lilac Lane, Alexandria VA 22308).

Green, A.W, 1990, "Intermagnet, A Prospectus", proposal for global real-time digital geomagnetic observatory network, distributed at First SESC Users Conference, Boulder, CO, 15-17 May 1990.

- Hill, T.W. and R.A. Wolf, 1977, "Solar Wind Interactions", in *The Upper Atmosphere and Magnetosphere*, Studies in Geophysics, National Research Council, NAS, Washington, D.C
- Jacobs, G. and T.J. Cohen (Editors), 1979, *The Shortwave Propagation Handbook*, Cowan Publishing Corp., Port Washington, NY.
- Jensen, D.C., R.W. Murray, and J.A. Welch Jr., 1960, "Tables of Adiabatic Invariants for the Geomagnetic Field, 1955.0", Air Force Special Weapons Center, Kirtland Air Force Base, New Mexico.
- Joselyn, J. et al., 1996, "Solar Cycle 23 Project: Summary of Panel Findings", NOAA-SEC panel of experts, sponsored by NASA.
- Jursa, A.S. (Scientific Editor), 1985, *Handbook of Geophysics and the Space Environment*, Air Force Geophysics Laboratory, Air Force Systems Command, U.S. Air Force, NTIS, Springfield, VA.
- Knecht, DJ. and B. M. Shuman, 1985, "The Magnetic Field", in *Handbook of Physics and the Space Environment*, edited by A.S. Jursa, AFGL, available through NTIS, Springfield, VA.
- Koons, H.C., and D.J. Gorney, 1990, "A Sunspot Maximum Prediction Method Using a Neural Network", *EOS*, AGU Trans., 71(18)677.
- Mayaud, P.N., 1980, *Derivation, Meaning, and Use of Geomagnetic Indices*, American Geophysical Union, Washington, DC.
- Meier, R.R., 2000, "Aeronomy and Space Weather: "Space Weather Effects and Metrics", article in *The CEDAR Post*.
- NOAA-NWS, 2004, "Intense Space Weather Storms October 19 – November 07, 2003", Service Assessment, U.S. Department of Commerce, NOAA, National Weather Service, Silver Spring, Maryland.
- Shea, M.A., SA Militello, H.E. Coffey, and J.H. Allen, 1984, *Directory of Solar-Terrestrial Physics Monitoring Stations*, Edition 2, MONSEE Special Publication No.2, published jointly by AFGL (Hanscom AFB, Bedford, MA.) and WDC-A for Solar-Terrestrial Physics (NGDC, NESDIS, NOAA, Boulder, CO.) under aegis of SCOSTEP, AFGL-TR-84-0237, Special Report No.239.
- Sheeley, N.R. Jr., J.W. Harvey, and W.C. Feldman, 1976, "Coronal Holes, Solar Wind Streams, and Recurrent Geomagnetic Disturbances, 1973-1976", *Solar Physics*, 49:271.
- Sheeley, N.R. Jr., and J.W. Harvey, 1978, "Coronal Holes, Solar Wind Streams, and Geomagnetic Activity During the New Sunspot Cycle", *Solar Physics*, 59:159-178.
- Simpson, S., 2003, Massive Solar Storms Inflict Little Damage on Earth", *Space Weather Journal*, 2003SW000042, 28 November 2003.

- Tsurutani, B.T., W.D. Gonzalez, Y. Kamide, and J. Arballo (editors), 1997, *Magnetic Storms*, AGU Geophysical Monograph 98, American Geophysical Union, 2000 Florida Avenue, Washington DC 20009.
- Stewart, F.G. and M. Leftin, 1972, "Relationship Between the Ottawa 10.7 cm. Solar Flux and Zurich Sunspot Number", *Telecommunications J*, 39:159-169.
- Valley, S.L., (editor), 1965, *Handbook of Geophysics and Space Environments*, Air Force Cambridge Research Laboratories, Office of Aerospace Research, USAF, Hanscom AFB, Bedford, MA.
- Whalen, J.A., R.R. O'Neil, and R.H. Picard, 1985, "The Aurora", in *Handbook of the Geophysics and the Space Environment*, edited by A.S. Jursa, AFGL, USAF, NTIS, Springfield VA.
- Withbroe, G.L, 1989, "Solar Activity Cycle: History and Predictions!", *J.Spacecraft and Rockets*, 26:394.



<http://www.springer.com/978-0-387-23670-4>

Space Weather & Telecommunications

Goodman, J.M.

2005, XX, 382 p., Hardcover

ISBN: 978-0-387-23670-4